Technical Reviews

Optical vegetation indices for monitoring terrestrial ecosystems globally

Yelu Zeng [a], Dalei Hao [b], Alfredo Huete [c], Benjamin Dechant [d], Joe Berry [e], Jingming Chen [f], Joanna Joiner [g], Christian Frankenberg [h,m], Ben Bond-Lamberty [i], Youngryel Ryu [j], Jingfeng Xiao [k], Ghassem R. Asrar [l], Min Chen [a]

[a] Department of Forest and Wildlife Ecology, University of Wisconsin-Madison, 1630 Linden Drive, Madison, WI, USA

[b] Atmospheric Sciences and Global Change Division, Pacific Northwest National Laboratory, Richland, WA, USA

[c] School of Life Sciences, University of Technology Sydney, Sydney, NSW, Australia

[d] Synthesis Centre for Biodiversity Sciences, German Centre for Integrative Biodiversity Research, Puschstraße 4, 04103 Leipzig, Germany

[e] Department of Global Ecology, Carnegie Institution for Science, Stanford, CA 94305, USA

[f] Department of Geography and Program in Planning, University of Toronto, Toronto, ON M5S 3G3, Canada

[g] NASA Goddard Space Flight Center, Greenbelt, MD, USA

[h] Division of Geological and Planetary Sciences, California Institute of Technology, Pasadena, CA, USA

[i] Joint Global Change Research Institute, Pacific Northwest National Laboratory, College Park, MD 20740, USA

[j] Department of Landscape Architecture and Rural Systems Engineering, Seoul National University, South Korea

[k] Earth Systems Research Center, Institute for the Study of Earth, Oceans, and Space, University of New Hampshire, Durham, NH 03824, USA

[l] Universities Space Research Association, Columbia, MD 21046, USA

[m] Jet Propulsion Laboratory, California Institute of Technology, Pasadena, USA
Corresponding authors: Min Chen (mchen392@wisc.edu) and Dalei Hao (dalei.hao@pnnl.gov)

Key points

- Optical vegetation indices (VIs) derived from space-borne Earth observations are widely used for monitoring terrestrial ecosystems including plant biophysical, biochemical and physiological properties, vegetation dynamics and environmental stresses.
- Sensor and calibration effects, quality assurance and quality control (QA/QC) flags, bidirectional reflectance distribution function (BRDF), atmospheric and topographic effects, and snow/soil background are among important sources of VI-based uncertainties.
- Potential artefacts must be carefully considered to avoid biased interpretations of the underlying ecological processes resulting from the improper use of VIs.
- VIs based on ratios of reflectance such as NDVI can help reduce sensor calibration, BRDF, atmospheric and topographic effects, but could be sensitive to snow/soil background and scale effects.
- NIRv has the biophysical meaning of FPAR times the photon escape ratio (*fesc*), and is linearly correlated with EVI, EVI2 and DVI on a mathematical-basis, while ratio-based NDVI behaves differently.
- Next generation VIs with greater signal sensitivity and less artefacts, are expected with new hyperspectral/geostationary satellite missions and synergistic integration with other metrics, providing advanced opportunities for studying terrestrial ecosystems.

Abstract

Vegetation indices (VIs) are widely used in studying vegetation dynamics across spatial (local, regional, and global) and temporal (sub-hourly, daily, seasonal, annual, and decadal) scales. However, diverging conclusions have often been reached for the same canopy conditions using different VIs, rendering past and present scientific studies by the ecological community ambiguous. In this review, we summarize the rationale, history and ecological applications of VIs, and provide useful insights on VI inconsistencies due to improper considerations of a variety of factors, such as the use of different VIs, sensors, satellite product versions, atmospheric and sun-target-sensor geometry corrections, compositing algorithms, and use of quality assurance and control (QA/QC) flags. The debate on Amazon forest greening in the dry season is used as an example to illustrate VI inconsistencies. We demonstrate that the photon escape ratio (*fesc*) from the canopy provides the mathematical- and physical-basis for the intrinsic linkage among several of the most widely used VIs. NIRv, EVI, EVI2 and DVI are strongly linearly correlated with each other while NDVI behaviors differently. Identifying key sensitive wavelengths for target application is the first step towards the optimal use of VIs, followed by an understanding of potential signal contamination sources in the specific ecosystem.

1. Introduction

Vegetation indices ('VIs') are simple mathematical combinations or transformations of reflectance in two or more spectral channels to represent vegetation status conditions (Fig. 1), while minimizing the impacts of other contributing factors such as the soil background, atmosphere and sun-target-sensor geometry[1-3]. As useful and efficient tools, VIs have attracted a large community of users from a wide range of scientific disciplines over the last half century. VIs are also easily obtained at different scales, from the ground with hand-held spectral sensing devices, tower-based and airborne sensors up to satellites, and hence can provide measurements from the fine to coarse resolutions. VIs are highly objective, with no or only minimal assumptions with regard to land cover type and canopy structure. As a result, they have been intensively used in local to global scale studies, and in almost every discipline of Earth science, especially in ecological research[4-6].

A number of VIs have been developed since the early 1970s (Table 1). Many of them can be easily calculated from publicly available remote sensing data, while the subtleties in processing and interpretation of results require more experience and theoretical background. With their wide adoption, VIs are increasingly applied to more challenging research questions/experiments to shed light on complex ecological topics such as vegetation response to long-term climate change[7-9], short-term disturbances[10,11] and extreme climate events[12]. The simplicity of VIs, however, can be deceptive as there are many cases of confusion, misinterpretations, and scientific controversies related to their use.

This review aims to inform scientists with the rationale, history, and key features of VIs that hopefully can be helpful for better understanding and using VIs for ecological studies. Although hundreds of VIs have been proposed, there is no necessity to go through all these VIs because many of them were built with similar formulae or principles. Instead, we will reinvestigate a selected subset of the most widely used VIs in this review, with a particular emphasis on clarifying and summarizing their usefulness, relationships, inconsistencies, artefacts and limitations. We also attempt to present recommendations on how to avoid these potential pitfalls to improve their use for the wider ecological community. In addition, since most existing VIs are based on reflectance in the optical wavelengths, we mainly focus on the optical VIs in this review, and particularly on those having the potential to be derived by satellite observations and applied globally. We use a few 'milestone' VIs as representative examples across our technical analyses, such as the Normalized Difference Vegetation Index (NDVI), the Enhanced Vegetation Index (EVI), and the Near-Infrared Reflectance of Vegetation (NIRv), which are among the most widely used VIs in a variety of global-scale ecological studies and can reveal some common features of many VIs.

2. Rationale of VIs

The launch of Earth observing satellites since 1972 ushered a new era for global observation and study of vegetation (Fig. 2)[13]. The physical foundation of VIs, as a product of the remotely-sensed spectral reflectance, is built on our understanding of the complex light-vegetation interactions. Essentially, satellite-measured spectral reflectance is a mixed signal of vegetation canopies, their shadows, soils and possibly other components standing on the land surface, and is commonly co-determined by leaf reflectance, the background soil reflectance, canopy structure, and the sun-sensor geometry. The spectral signature of leaf reflectance is well understood (Fig. 1). Leaf reflectance is relatively lower in the visible (VIS) domain (400~700 nm) because of the strong absorption of photosynthetic pigments, particularly in the non-green wavelengths due to the absorption of chlorophylls; high leaf reflectance in the near infrared band (NIR; 700~1300 nm) is usually expected due to spongy mesophyll, and lower leaf reflectance happens in the shortwave infrared (SWIR; 1300~2500 nm) due to strong water absorption and, to a less degree, other leaf biochemical traits such as lignin, protein and cellulose content. A typical soil reflectance spectrum monotonically increases with wavelength in the optical domain except the water absorptions in the SWIR band. Canopy structure is a key factor for the canopy reflectance, because it determines how much of the incoming light is reabsorbed, re-scattered and finally escapes from the canopies. Biophysical or structural parameters such as Leaf Area Index (LAI), Leaf Angle Distribution (LAD) and Clumping Index (CI) are commonly used to characterize canopy structure. The sun-sensor geometry further complicates the canopy reflectance observations, largely due to the fraction of shadows in view because of the varying relative positions of the light source (sun) and the sensor. Furthermore, the atmospheric radiative transfer process is another important factor to consider in practice.

Therefore, VIs have been developed based on the simple rationale that the spectral signals from the vegetation, and more specifically, the vegetation characteristics of interest (for example, vegetation biophysical, biochemical and physiological properties) should be enhanced with properly designed mathematical combinations such as ratios, differences, derivative, or the combinations of the ratios and differences between reflectance from different spectral wavelengths or bands (Fig. 3). This enhancement goes along with reducing, or ideally suppressing background signals from soil and confounding factors related to vegetation characteristics with overlapping spectral features. However, even for a given vegetation characteristic, it is not straightforward to use one single formula that holds under different conditions. This, together with the interest in various different vegetation characteristics as well as increasing availability of more and more and increasingly narrow spectral bands from satellite sensors, is driving the continuing development of VIs.

3. A Brief History of VIs

3.1 VIs for plant biophysical properties

The history of VI developments goes back to the early 1970s (Fig. 2). The first-generation red-NIR ratio- and difference-based VIs, including the Simple ratio (SR), Difference Vegetation Index (DVI) and NDVI[14-16] were proposed to quantify vegetation growing condition based on the fact that live green vegetation significantly absorbs solar radiation in red but reflects most of the solar energy in NIR to support photosynthesis while avoiding potential damage from overheating[17] (Fig. 1). Further refinements have been introduced to minimize the effects of intervening soil background and atmosphere to better isolate the vegetation contributions, especially for sparse vegetation cover[1,18]. Examples include an orthogonal-transformation based perpendicular vegetation index (PVI)[19], the soil adjusted vegetation index (SAVI)[3], Transformed SAVI (TSAVI)[20] and Modified SAVI (MSAVI)[21]. Later, Modified Simple Ratio (MSR)[22] was formulated based on the evaluation of several two-band VIs (for example, SR, NDVI and SAVI) for the purpose of improving the linear relationship with biophysical parameters and reducing the sensitivity to measurement noise[22]. Reduced SR (RSR) further increased the sensitivity and correlation to LAI than SR, and reduced the effect of background reflectance by taking the canopy closure and understory contribution of open canopies into account with the SWIR band included[23].

The Global Environment Monitoring Index (GEMI) was introduced to reduce the atmospheric effects[24]. The launch of MODIS onboard NASA's Terra and Aqua satellites in the early 2000s opened new opportunities for VI developments with more spectral bands in the optical wavelengths. The Atmospherically Resistant Vegetation Index (ARVI) and EVI[25] were proposed to minimize the atmospheric effects with an expected blue to red band 'atmosphere scatter' signal, enabling correction from the blue and red band relative proportions[25,26]. As atmospheric correction algorithms improved, the two-band version of EVI (EVI2)[27] with the absence of the blue-band was developed in 2008 without blue band while achieving similar performance as compared with EVI[27]. In 2014, plant phenology index (PPI)[28] was derived for estimating plant canopy growth, especially for evergreen forest phenology over high latitudes[28]. PPI has a nearly linear relationship with green LAI, and soil brightness variations have moderate impact on PPI. More recently, NIRv[4] and the fluorescence correction vegetation index (FCVI)[29] were added to the list because of their ability to reduce soil background effects on the NIR reflectance of vegetation and to better approximate the vegetation's solar radiation absorption and photosynthesis[4,30]. NIRv has received significant attention and application because of its clear physical foundation and strong correlation with vegetation photosynthesis (Fig. 3)[4,30]. In 2021, the kernel NDVI (kNDVI) was proposed based on the theory of kernel methods as a unifying VI for monitoring the terrestrial carbon dynamics and increasing the sensitivity of NDVI to plant biophysical parameters[31].

3.2 VIs for plant biochemical properties.

Broad-band reflectance smooths the detailed spectral signatures and thus above-mentioned broad-band VIs are primarily designed for detecting vegetation structure and its changes. In parallel, a group of VIs were developed by taking advantage of narrow-band sensor measurements that keep more detailed spectral information. In general, narrow-band VIs are specifically designed to indicate the biochemical and physiological properties such as pigments, water, plant residues and nitrogen[32], and typically use a combination of strong-absorbing VIS bands and a narrow band located in the red-edge region (670~780nm). Examples include Red Edge Chlorophyll Index (CIred-edge)[33], Red-edge NDVI (NDVIre)[34] and MERIS Total Chlorophyll Index (MTCI)[35] for indicating chlorophyll content, the Structure Insensitive Pigment Index (SIPI)[36], Normalized Pigments Chlorophyll Ratio Index (NPCI)[37], Plant Senescence Reflectance Index (PSRI)[38] for carotenoid content, and Anthocyanin Reflectance Index (ARI)[39], Anthocyanin Content Index (ACI)[40] and Red/Green Ratio Index (RGRI)[41] for anthocyanin content. Using the water absorption bands around 970, 1200, 1450, 1940 and 2500 nm, Normalized Difference Water Index (NDWI)[42], Land Surface Water Index (LSWI)[43,44], and Normalized Difference Infrared Index (NDII)[45] were designed with a similar formula and exhibit similarly robust performance on indicating vegetation hydrological condition[46]. The Normalized Difference Lignin Index (NDLI) was designed with the 1754 nm lignin absorption feature, and the Normalized Difference Nitrogen Index (NDNI) considered the 1510 nm nitrogen absorption feature[47].

3.3 VIs for plant physiological properties

Another group of VIs were proposed to detect stress-induced physiological changes in xanthophyll cycle pigments, as indicators of photosynthetic light use efficiency or environmental stresses[48]. Because the reflectance at 531 nm is sensitive to carotenoid pigments and the xanthophyll cycle, the Photochemical Reflectance Index (PRI) was proposed (with a reference wavelength at 570 nm) in 1992 to track changes in diurnal photosynthetic efficiency[49]. The Chlorophyll/Carotenoid Index (CCI) proposed in 2016 is another index for representing the dynamics of the chlorophyll/carotenoid ratio and has the potential to track seasonal variations of canopy photosynthesis at the global scale[5], because it could be directly obtained from existing satellite data. PRI, CCI and green chromatic coordinate (GCC) can capture the seasonal variation of carotenoid and xanthophyll cycles over temperate evergreen needleleaf forests that are difficult to detect with broadband VIs such as NDVI and NIRv[50,51]. Red-edge Vegetation Stress Index (RVSI)[52] had less negative values for stressed leaves than healthy leaves in grapevine leafroll disease detection over two wine grape cultivars[53].

3.4 Satellite sensors for VIs

VIs can be calculated from reflectance measurements by a series of Earth-observing satellite sensors[13] (Fig. 2). Landsat 1~3 MultiSpectral Scanner (MSS) since 1972 only had four VIS-NIR bands with about 80-m spatial resolution and half-monthly revisit cycle, while since Landsat 4 was launched in 1982, the spatial resolution in VIS-NIR bands has increased to 30-m. Sensors with similar spatial resolution include SPOT (1986~) and Sentinel-2 (2015~), which have weekly to daily temporal resolution. Sentinel-2 is one of the few sensors with the capability to calculate red-edge VIs for plant pigments. AVHRR, MODIS and VIIRS, launched in 1981, 1999 and 2011, respectively, have the daily temporal coverage, while AVHRR does not have the blue band for EVI. Towards high temporal resolution, geostationary satellites, such as GOES and Himawari both launched in the 1970s, had sub-hourly VI observations. NDVI, SR and RSR have been employed to generate global LAI products from Himawari, AVHRR and MODIS observations with biome-specific LAI-VI relationship[54-56], while global leaf chlorophyll content was firstly generated from MERIS observations by physically-based radiative transfer models instead of the chlorophyll-sensitive MTCI, due to the impact of LAI on MTCI[57]. For very high spatial resolution (<10-m), GeoEye-1, WorldView 2-4, Pleiades, SkySat and PlanetScope are available since 2009 but can only provide VIS-NIR reflectance for vegetation biophysical properties. DESIS and HiSUI on the International Space Station, and as well as Hyperion and PRISMA, provide the hyperspectral observations while they just have monthly revisit cycle on average, which are suitable for plant biochemical and physiological traits mapping instead of capturing rapid temporal changes of vegetation.

4. Ecological applications of VIs

VIs have been successfully applied to many specific ecological research fields. Below we discuss a few prototypical examples.

4.1 Estimating vegetation attributes

An essential attractive feature of VIs is their conceptual simplicity and strong relationships with vegetation biophysical properties. Therefore, using VIs to estimate vegetation biophysical properties such as LAI, fractional vegetation cover, and biomass[54,55,58] is one of the most successful application scenarios. Many VIs such as NDVI have been used as robust estimators of LAI and fractional vegetation cover. A few problems of NDVI are well identified, such as the insensitivity to densely vegetated areas and the oversensitivity to the changes of soil brightness due to rainfall and snowfall. The saturation point of EVI is higher than NDVI[25,27], leading to more EVI applications in densely vegetated area like tropical forests. In particular, chlorophyll-corrected VIs can minimize the impact of chlorophyll content on LAI estimations. For example, a modified triangular vegetation index (MTVI2) and a modified chlorophyll absorption ratio index (MCARI2) have shown to be the best predictors of green LAI in a systematic evaluation of more than ten VIs (including NDVI, MSR, SAVI, etc.) over various crops[59].

For vegetation biochemical properties (Table 1), red-edge VIs have been widely used for estimating leaf/canopy chlorophyll content and carotenoid pigments[60], while SWIR-based VIs were often roughly used for leaf/canopy water content, leaf mass per area and (LMA) and nitrogen estimations[32]. These retrieved plant traits can be directly used to quantify the functional diversity, while the spatial distribution and textural feature of VIs such as MODIS EVI have also been applied in studying the spectral diversity, species richness and habitat heterogeneity[61,62].

4.2 Temporal vegetation dynamics

Compared to other VIs, NDVI and EVI are the most widely used ones in practice for detecting and monitoring temporal vegetation dynamics because of their simplicity, robustness and availability, especially for the seasonal (phenology) and long-term trends of structural changes [7,63-

[65]. EVI and EVI2 are the primary data source for producing the MODIS vegetation phenology product Collections 5 and 6, respectively. In the recent years, NIRv is gaining popularity for analyses of vegetation changes regarding the ecosystem gross primary production (GPP)[66]. PPI and EVI2 performed better than NDVI with Sentinel-2 imagery across Europe when compared to ground-observed phenological stages, especially for evergreen coniferous forest during winter with snow[67]. CCI better tracked evergreen forest phenology and the end-of-season changes in deciduous forests compared to structurally-oriented NDVI, EVI and NIRv[68].

Artifacts such as sun-sensor geometry and inter-sensor calibrations usually play a critical role for correctly using and interpreting the results of VI-based temporal vegetation dynamics. During the past decades, considering the inter-sensor consistency and the sun-sensor geometry has been well recognized by the research community although different VIs may subject to such artifacts at different levels of sensitivities as discussed in Section 5.

4.3 Environmental stresses and disturbances

The abrupt temporal changes of VI time-series are also useful for the detection of land cover change, environmental stress and disturbance. EVI has been widely used to monitor and quantify the deforestation and degradation in the Amazon tropical rainforest[69], as well as the responses to drought, heatwave and water stresses[10,11,70]. Using PRI, CCI and GCC infers more seasonal physiological changes of vegetation than using structurally-oriented VIs such as NDVI and EVI in dormant temperate forests[50,51]. Biochemically-related VIs such as SIPI, NPCI and ARI have also been applied for the detection of pests and diseases in winter wheat[71], and the soil erosion and heavy metal pollution in rice[72], especially when hyperspectral data are available. Forecasting wildfire risks, monitoring fire severity, and characterizing vegetation recovery after fire disturbance is typically achieved by simple VIs such as NDVI, while hyperspectral imaging spectroscopy and light detection and ranging (LiDAR) are encouraged to be used in combination for the assessment of fuel condition and vegetation structure mapping[12]. NDVI has also been used for the assessment of ecosystem integrity and land degradation/desertification at different scales, including the resilience of agroecosystems[73].

4.4 Ecosystem carbon and water fluxes

Vegetation dynamics drive changes of surface radiation regime, which co-determine microclimate and land-atmosphere carbon and water fluxes, and thus has been an important application of VIs, in principle by employing VIs as the proxy for vegetation canopy coverage, leaf area and fraction of absorbed solar radiation (FPAR) (Fig. 3). FPAR is usually considered as a function of LAI, and thus the advantages and disadvantages of the VIs for monitoring LAI also apply to the carbon fluxes estimations.

Some notable examples of using VI to estimate carbon fluxes, particularly GPP, include the Carnegie-Ames-Stanford Approach (CASA)[74], MODIS algorithm[75] and EC-LUE model[76] (all using NDVI-derived FPAR); Vegetation Photosynthesis Model (VPM)[44], the modified GPP model in TEM[77], data-driven GPP upscaling[78] (using EVI); simpler statistical upscaling using NIRv[30,79]; regional forest GPP estimations[80] (using EVI2); satellite-based GPP with inexplicit parameterization of LUE[6,79] (using NDVI and soil-adjusted NIRv, SANIRv). All these approaches have demonstrated moderate to high success. NIRv has received growing attention in recent years because of its explicit physical link to FPAR[30,81,82] as well as a moderate relationship with LUE[83]. PRI, CCI and GCC are also found to well track the seasonal GPP dynamics, it is still challenging to establish quantitative relationships between these VIs and LUE for robust GPP estimations. Nevertheless, the inclusion of PRI together with NDVI had shown improvements in estimating boreal forest CO_2 fluxes [84].

VIs have been used as direct indicators of photosynthesis in studies, such as for examining the CO_2 fertilization effects by using AVHRR and MODIS NIRv[85,86], the carbon loss in Amazon rainforest degradation and deforestation with MODIS EVI[69], the change velocity and optimum air temperature of productivity across biomes by MODIS NDVI and NIRv[87], and the anomalies and recovery of the tropical forest during the strong 2015/2016 El Ni˜no event also with MODIS EVI[88,89]. Estimating belowground carbon fluxes from satellite observations has rarely been attempted and is based on indirect correlations between GPP and soil respiration via VIs[90].

Typically, NDVI, EVI and MSAVI were used as scaling factors to extrapolate field-level soil respiration measurements to larger scales [90,91].

Another prominent application of VIs is in the estimation of evapotranspiration (ET) with a history of over 30 years[92,93]. Although ET has been more accurately assessed using land surface temperature (LST), VIs are easier to obtain. The principle is because transpiration through plant leaf stomata generally dominates evaporation. A number of previous review papers have summarized that VIs in remote sensing ET models are powerful indicators of the fraction of vegetation coverage, absorption of solar energy, or surface roughness that are major determinant of ET[94,95]. Besides, due to the good VI-LST or VI-ET correlations observed at the flux tower sites in a wide variety of ecosystems, VIs have been used for either up-scaling site observation or enhancing/downscaling satellite LST, especially when LST data is unavailable or has a coarse resolution[94,96]. NDVI, SAVI and EVI are so far the most widely used VIs in a variety of ET estimation models[95-97]. However, due to NDVI's sensitivity to soil brightness, the more soil-resistant VIs, such as EVI, EVI2, NIRv and SAVI, are considered as better choices[92,94,96].

5. Artefacts that cause inconsistencies

VIs can be easily acquired from a variety of satellite sensors, however, inconsistencies in VI-based results reported in literature are common. Some of these inconsistencies are due to the use of different VIs, and a majority others are due to the artefacts of VI products derived from different sensors, satellite product versions, atmospheric and directional correction effects, compositing algorithms, and the application of different levels of quality assurance (QA) and quality control (QC) flags[70]. A comprehensive understanding of these inconsistencies as well as the limitations and caveats of each VI is critically important for rigorous use of VI and for the correct interpretation of the results from VI-based analyses. In this section, several notable examples of how VIs are not used consistently are discussed and classified by the primary factors for such inconsistencies (Fig. 4).

5.1 Sensor and calibration effects

There are inconsistencies in different satellite time-series for the same study area/region. For example, vegetation greenness trends derived from AVHRR and MODIS NDVI time series apparently show trends in opposing directions[98]. The differences in the central wavelength and range of the spectral response function across sensors can be important contributing factor for such inconsistencies[99,100]. For example, NDVI obtained from AVHRR, MODIS, and VIIRS show significant differences in values and the level of the differences varies across land cover types, although their orbits and spatio-temporal resolutions are similar[9].

Besides, satellites and their sensors often suffer from the harsh space environment, resulting in orbital drift and sensor degradation over time. Although onboard calibration or vicarious calibration are applied to maintain the measuring standards, the remaining limitations can affect the accuracy of the derived VIs and introduce systematic biases especially in long-term trend analyses[101,102]. Typical examples involve products from AVHRR and MODIS[103,104]. AVHRR measurements come from a series of satellites, each of which has specific orbital characteristics[105,106] which can affect the image acquisition time and sun-target-sensor geometry[104]. In particular, NDVI values from AVHRR onboard NOAA-11 were found to be significantly higher than those from prior and subsequent AVHRR sensors[107]. Orbital drift effects were also found in the VIP3 and LTDR4 NDVI data and over the more humid areas for GIMMS-3g NDVI. MODIS-based NDVI exhibited an increasing trend during 2001~2016, while a decreasing trend of the GIMMS-based NDVI was observed especially after 2012, which suggests large discrepancies of global greening[108]. A significant positive jump in the SPOT-VGT NDVI time series was identified due to the platform/sensor change from VGT-1 to VGT-2[8]. A recent study used AVHRR NIRv as a long-term consistent record to quantify the trends in CO_2 fertilization effect on global vegetation photosynthesis from 1982 to 2015[85]. However, concerns were raised about potential uncertainties in the conclusion partly due to sensor differences[86,104].

Another important issue is that different VIs may show varying levels of sensitivity to sensor calibration due to their mathematical formulae. The calibration bias may affect both VIS and NIR bands in a similar way, and thus can at least partly cancel out in ratio-based VIs such as NDVI and

SR. For example, the single-band reflectance calibration uncertainty for MODIS was 2% under normal atmosphere conditions, while the mean NDVI uncertainties due to sensor calibration was only ± 0.01 units and was less than 2% of the dynamic range using field canopy reflectance observations[109]. The cross-sensor difference of NDVI could also be smaller than the difference of surface reflectance. For the comparison among fifteen moderate-resolution sensors including MODIS, VIIRS and AVHRR, each pair of the sensors had a larger R^2 and smaller Root Mean Square Error (RMSE) for NDVI than for the VIS and NIR bands separately[9]. In VIs such as NIRv (=NDVI×NIR), such calibration biases do not cancel out and thus can impact the absolute values of the VI signals as NIR reflectance is multiplied. While this could be problematic for applications that rely on the absolute values of VI, it could also be an issue for the consistency of long-term time-series when there are differences in calibration bias between different sensors, or calibration drift of a given sensor over time. Therefore, differences in vegetation trends and magnitudes for different VIs can be due not only to the inherent characteristics of the VIs but also to their different sensitivities to calibration bias.

5.2 Product versions

VIs satellite products are usually produced in different versions (collections) with algorithmic improvements and calibration adjustments. Using different VI product versions may lead to inconsistent interpretation of changes in the vegetation. There still exist inconsistent greening/browning trends between MODIS Collection 5 (C5) and Collection 6 (C6) products[102]. MODIS itself suffers from sensor degradation, which is the largest for the Terra satellite especially in the blue band[102,110]. The degree of degradation decreases with increasing wavelength, and thus there are negative decadal trend artefacts for MODIS Terra products with △NDVI~0.01 and △EVI~0.02[110] when comparing C5 to an enhanced C6 (C6+) version. The percentage of negative MODIS-C5 NDVI trends derived from Terra (17.4%) was nearly three times as large as that derived from Aqua (6.7%) for North America during 2002~2010[101]. Most of the vegetation browning trends revealed by MODIS Terra-C5 VIs were likely caused by sensor degradation, particularly during the period after 2007, and thus previous studies of vegetation trends based on only Terra-C5 VIs may need to be re-evaluated[102]. Thus the latest MODIS C6 has sensor degradation corrected and better consistency between Terra and Aqua measurements and provides a more reliable record than C5[110].

5.3 Pre-processing steps

Standard VI products usually include important data pre-processing and sensor configuration information, such as the sun-target-sensor geometry and QA/QC, which if not taken into account appropriately, could introduce critical errors in the subsequent analyses. The relative positions of the sun, sensor and observing target commonly change over time due to the continuous movement of Earth, sun, and satellites. Such changes result in the variations of the solar illumination and sensor viewing angles and have been recognized for decades to affect remotely sensed observations strongly[111-113]. This effect can be mathematically described as the bidirectional reflectance distribution function (BRDF) effect or the sun-target-sensor geometry effect (Fig. 4).

The solar angle is seasonally and latitudinally varying but annually repetitive if a sensor remains in a stable orbit, and therefore it can influence the VI-based phenology, but not the long-term trends or interannual variations. For example, Amazon forests have been reported to exhibit no variations in EVI from wet to dry season, and dry season greening has been attributed to seasonal solar-angle variations[112]. Subsequent studies using either the same data[114] or the rigorously BRDF-corrected MAIAC product[115] suggested dry-season greening but with smaller magnitude, which demonstrates the importance of disentangling solar angle-induced seasonal variations in VI from vegetation-induced variations. A similar case also shows that the BRDF effect, instead of the vegetation response, drives the satellite NDVI phenology in evergreen sparse canopy ecosystems in western US with subtle growth dynamics[116]. Not only MODIS, but also Landsat 7, Sentinel-2, VIIRS and Proba-V confirmed this effect with the ground-based PhenoCam observations as the reference. Thus the authors suggest to either restrict the analyses to selected data with consistent sun-target-sensor geometry, or to rigorously remove the BRDF effect in the data[116]. Landsat that only acquires images at ± 7.5° from nadir has relatively small view angle effects[117], while other satellite sensors such as AVHRR and MODIS usually extend to larger view angles, which can introduce uncertainties to the downstream products if uncorrected[111,113]. The impact of the BRDF effect on MODIS NDVI was evaluated in West Africa, and was found to be the highest for medium dense vegetation (NDVI≈0.5~0.6) compared to sparsely canopy (NDVI≈0.3~0.35) or dense vegetation (NDVI≈0.7)[113]. In Alaska Arctic tundra, the influence of BRDF effect on satellite NDVI-based biomass estimations was up to 33% (excluding extremes) more sensitive than on NDVI[111].

A related uncertainty source is the compositing approach, which determines how to extract the highest quality observations over the typically used 8-day, 16-day, or monthly interval. Compositing has gone through major changes between the traditional Maximum Value Compositing (MVC) algorithm, which is still employed in GIMMS-3g datasets, to the modified constrained view angle MVC, or CV-MVC[25], used in MODIS VI compositing (MOD13A1 and MYD13A1), to the 16-day rolling compositing based on BRDF retrievals used in MCD43A4 Nadir BRDF-Adjusted Reflectance (NBAR)-VIs[118]. Note that MOD13A1 and MYD13A1 products with the CV-MVC algorithm aimed to reduce the BRDF effect but still did not theoretically normalize it[119], while the MCD43A4 C6 product removed the view angle effects but was set at the local solar noon zenith angle[120] which varies seasonally and latitudinally. Compositing approaches vary widely and can lead to inconsistencies in the interpretation of results. For example, in the studies conducted over the Amazon[63,70,121] and western US[116], selective compositing settings based on study objectives resulted in inconsistent results.

Another source of inconsistency is the atmospheric correction, which was either conducted fully, partially or sometimes not at all conducted for different VI products. MODIS attempted the full correction, while GIMMS attempted at limited correction. NDVI derived from VIIRS observations is based on top-of-atmosphere (TOA) reflectance, while VIIRS EVI is generated based on surface reflectance[122]. Even when VIs are calculated from atmospherically-corrected reflectance at the surface, they are still subject to uncertainties in atmospheric correction such as cloud masking, residual sub-pixel clouds, incomplete corrections for Rayleigh scattering, ozone, water vapor absorptions, and imperfect aerosol correction[123]. In the studies regarding the impact of drought on Amazon forests, where VIs were intensively used, large differences were found in the extent of Amazon greening during the 2005 drought that were attributed to inadequate QA/QC screening for clouds and aerosols effects that are usually accounted for in atmospheric correction process[70].

5.4 Soil, snow and topographic effects

Most of Earth's terrestrial ecosystems have sparse canopies with appreciable canopy background (soil, litter, snow, water, etc.) signals that can affect satellite-derived VIs. Soil types and soil moisture conditions lead to spatiotemporal variations of soil brightness[124]. In natural ecosystems, the soil layer could be mixed with litter, moss, lichen, or waterbodies; and especially in forest ecosystems, woody stems and branches could contribute to the background noise or bias of VIs[125]. Soil influences are assumed to vary the most in arid regions, while they have the greatest effect in moderately vegetated canopies (LAI ~1 or ~50% cover). For example, in northern Africa, extensive soil-artefacts in the AVHRR-NDVI signals are seen over reddish soils[126], while in the Sahel, the NDVI variations were reported due to soil type, moisture and reflectance differences[127]. The first rains can result in an artefact NDVI flush prior to the actual greening cycle, while over-irrigated and freshly ploughed croplands, one can see similar NDVI 'soil artefacts'[128]. Snow and ice with high optical reflectance are among the most important factors that lead to the inconsistency of the VI time-series during winter in temperate regions[116,129] or, more permanently, in Arctic[130]. There is evidence of bias in the detection of vegetation phenology phase using NDVI at the end of non-growing season, due to presence of snow that causes low NDVI values[131].

In addition to soil and snow, topography also influences VIs. Mountainous regions cover 24% of the total Earth's land surface[132]. Topography, which can cast macro-scale shadows and change the local sun-surface-sensor geometry, has been reported to have important effects on surface reflectance[133] and VIs[134]. Similar to the shadows in view caused by the sun-target-sensor geometry, a topographic shadow is much darker in the red wavelength than in highly scattered NIR wavelength due to the multiple scattering between slopes[135]. Compared to the sun-target-sensor geometry-induced porous and fuzzy canopy shadows, the dark and opaque topographic shadows can have larger effects on EVI[134]. The topographic effects on reflectance should be minimized before EVI and other VIs without a band-ratio format (such as NIRv and SAVI) are calculated, while the topographic effects on the ratio-based VIs such as SR and NDVI are usually smaller[134]. The topographic effects are also related to the spatial scale and as the size of the pixel increases, the topographic effects may decrease and even disappear with spatial averaging[136].

5.5 Scale-mismatch effects

Spatial mismatches between the region-of-interest and the predefined grid cells in the remote sensing-based datasets could be another important source of uncertainty[137]. For example, MODIS pixels have accurate geolocation, yet on average, the offset is up to half a pixel between scenes, which is significant when users rely on single pixel VIs to match with *in-situ* measurements[138]. Considering that the *in-situ* measurement is rarely near the centre of a pixel, there is high probability that a single MODIS pixel may not always sample the *in-situ* measurement area. The sensor point spread function could further distort the matching of gridded satellite data with ground-based data[137]. The emerging high-spatial resolution data (for example, PlanetScope and airborne data, ≤ 3 m) could also lead to difficulties in the interpretation. For example, a pixel could be completely in the shadows of a tree so that VI values could be highly distorted due to the lower illumination than sunlit crown side if the research target is the whole tree canopy[139]. Identifying a suitable remote sensing product at an appropriate spatial scale could be the most effective choice for minimizing such uncertainties.

There is a general lack of studies that use long-term, well-coordinated *in-situ* networks to measure reflected radiation from vegetation to confirm larger scale greening and browning results. The MODIS EVI results related to the Amazon dry season greening were confirmed with *in-situ* measurements of GPP from eddy-covariance flux towers[140]. In contrast, the greening trends in the Sahel challenge the mainstream paradigm of irreversible ground-observed land degradation in this region[141]. There is also a debate as to whether the onset of spring phenology has been advancing due to climate warming. The trends in the Start Of growing Season (SOS) for Tibet alpine meadow and steppe were examined using ground-based phenology observations as well as NDVI datasets from GIMMS and GIMMS3g, MODIS, SPOT-VEG and SeaWiFS[142]. The results from that study showed large discrepancies in the SOS trends among the ground-based and different NDVI datasets, and between the different phenology retrieval. The study pointed out the NDVI data quality and scale-mismatch between satellite and ground data might be an important reason for these inconsistencies. Similar results were reported by comparing ground-based PhenoCam data with EVI derived from a variety of sensors including Landsat ETM+, MODIS, and DSCOVR-EPIC[65]. At three rural sites and one urban site of deciduous trees in Ireland, AVHRR and MODIS EVI2-derived SOS during 1982~2016 was consistently earlier than *in-situ* leaf-unfolding across all these sites with the RMSE of 25~52 days and Mean Bias Error (MBE) of −5 to −50 days, while satellite-derived growing-season-length was consistently longer than *in-situ* data with the RMSE of 65~102 days and MBE of 45 to 96 days[143]. For the period 2001~2014, MODIS EVI2-derived SOS advanced by about 2.36 days from middle to high latitudes of Northern Hemisphere (43.5°N~70.0°N) snow-covered landmass, while delayed by about 0.53 days in lower latitudes (33.0°N~43.5°N); the differences between MODIS EVI2-derived SOS and *in-situ* SOS at 420 phenology observations from five filed datasets including Pan European Phenology (PEP) project[144,145] are centralized between −30 days and 30 days, with the coefficient of determination (R^2) of 0.67, RMSE of 12.13 days and bias of −3.99 days[146].

6. Limitations and intrinsic linkage

6.1 Notable limitations of VIs

In principle, VIs capture a combination of canopy properties and other external contributing factors such as atmospheric conditions and sun-target-sensor geometry that may simultaneously and non-uniquely vary throughout the vegetation growing season. Thus, it might be infeasible to physically couple a VI to a specific plant variable without accounting for changes due to these factors and changing vegetation conditions at the same time. For example, a VI cannot be coupled to leaf biomass, without accounting for simultaneous differences in leaf biochemical constituent differences, non-photosynthetic vegetation (NPV), soil background, atmospheric contamination, and canopy structural effects, which are also tightly connected to the sun-target-sensor geometry effects. From the mathematical formula, a large group of ratio-based VIs (e.g., NDVI, SR, PRI, CCI and CIred-edge), are sensitive to different soil brightness due to the larger variation of the denominator than the numerator[2], but are insensitive to fractional vegetation cover when the soil background is dark or in water for mangrove[147]. For example, a leaf floating in a black water body would maintain the same NDVI regardless of how large the leaf became (whether that leaf occupies 1% of the water or 100% of the water, the NDVI is the same, as in Fig. 4).

Impacts of some inherent properties of vegetation, such as the leaf biochemical constituents and NPV, are usually difficult to separate because of limited understanding of their spatiotemporal variations. Leaf biochemical constituents, such as chlorophyll, water and dry matter contents, largely determine the leaf reflectance spectrum and thus fundamentally shape the vegetation canopy reflectance[148,149]. Recent studies have demonstrated the strong spatio-temporal variations of leaf biochemical constituents[57,150], which contribute to the important plant diversity but greatly complicate the interpretations of VIs. NPVs, such as woody stems, branches, and standing litter[151] can mask emerging green vegetation and thus can weaken the correlation between VIs and green vegetation biophysical properties. Therefore, satellite-derived phenology could be delayed due to the masking of NPVs, because the standing plant materials from the previous year may occlude the initial green-up of vegetation[151]. The limitations of VIs can be at least partially addressed when the VI formulae are appropriately designed with the principles of radiative transfer in vegetation canopies (Section S2.2).

6.2 Intrinsic similarities between VIs

Red-NIR VIs , such as NDVI, DVI, EVI, EVI2 and NIRv, are typically among the most widely-used category. In general, surface reflectance in NIR band is larger than that in the red band. In addition, canopy NIR reflectance essentially increases with LAI while red reflectance shows the opposite trend due to strong light absorption at this wavelength. Therefore, NIR typically dominates the factor NIR/(NIR+Red), which equals NIRv/DVI. It typically falls in a small range of 0.8~1 for vegetated surfaces (LAI>1). Therefore, Eq. 2 in Box 1 suggests that NIRv is well correlated with DVI in most cases, and NIRv has the biophysical meaning of FPAR times photon escape probability (*fesc*) (Fig. 3a).

EVI has been reported to be well approximated by EVI2, a variant of EVI without the blue band[27]. EVI and EVI2 can be derived as the product of DVI and 2.5/(NIR+6·Red+7.5·Blue+1) or 2.5/(NIR+2.4·Red+1) (Eqs. 3-4), respectively[27]. Note that the number '1' in the denominator is typically much larger than the variability of the remaining term (NIR+2.4·Red) or (NIR+6·Red+7.5·Blue) in response to the changes of LAI. Thus, the factor 1/(NIR+6·Red+7.5·Blue+1) (Eq. 3) is typically between 0.7~0.8 in most cases especially when LAI is greater than 1. Similarly, the factor 1/(NIR+2.4·Red+1) is also almost a constant with small variation between 0.7~0.8 in most cases. This suggests that EVI2 and EVI should have a strong linear correlation with DVI, although with different magnitudes because of the constant coefficient (2.5) used in the numerator.

Thus, DVI is strongly correlated to both EVI and NIRv, and NIRv, DVI, EVI and EVI2 intrinsically have strong linear correlations with one another according to their mathematical definitions and typical range of variation of NIR and VIS reflectance of vegetated surfaces. In contrast, DVI is mathematically the numerator of NDVI, and the denominator (NIR+Red) can vary significantly with LAI and other vegetation properties. Therefore, a nonlinear relationship is often observed between NDVI and DVI, and thereby also between NDVI and the other indices similar to DVI, such as EVI, EVI2 and NIRv.

NDVI, EVI and DVI can also be more generally described by another well-known VI, the SAVI, and the 'L' in the denominator of SAVI (Eq. 7) is the canopy background adjustment term that addresses the nonlinear, differential NIR and red radiative transfer process through a canopy[3,25]. In case L in SAVI is 0, SAVI is equal to NDVI; if L is 1, SAVI equals to EVI. Note that factors of 6 and 7.5 in the denominator of EVI (Eq. 3), and 2.4 in the denominator of EVI2 (Eq. 4), are for atmosphere self-correction instead of canopy biophysical properties. Third, when L is infinity, SAVI is equal to DVI. The real canopy has an L value generally greater than 0 but less than 10. Details about the evaluation of similarity and difference among these VIs, and their sensitivity to artefacts such as the impacts of soil background, atmospheric contamination, canopy structural and sun-target-sensor geometry effects are in Section S2.1.

7. Appropriate use of VIs

Attractive features of VIs are their conceptual simplicity and strong relationships with target properties of the vegetation and land cover. Because of the diverse types and application scenarios of VIs, it is not possible for a universal recommendation of the best VI. Instead, identifying the target application and corresponding sensitive wavelength and VI is the first step towards the optimal use of VIs. For example, red-NIR VIs such as NDVI and EVI may be the best choices for studying dynamics of vegetation structure, red-edge VIs are more suitable for pigment retrievals, while VIS-based PRI and CCI are more appropriate for the monitoring of physiological changes. Then, understanding the intrinsic differences, strengths and particularly the limitations of VIs may help to further identify the suitable VIs. For example, NDVI may be the best candidate VI for estimating fractional vegetation cover as it is less impacted by sun-target-sensor geometry than EVI and NIRv, while if the sun-target-sensor geometry effect is properly addressed, NDVI may be less robust in estimating fractional vegetation cover due to the stronger sensitivity to soil brightness changes from rainfall or snowfall[2,3]. In addition, VIs are typically saturated in dense vegetated areas; the saturation point of NDVI is usually lower than EVI[25,27], suggesting that NDVI may be a less appropriate choice for analysing vegetation variations in dense vegetation canopies, while NDVI is still useful for onset/offset phenology detection. Even though EVI, EVI2, DVI and NIRv show high correlations, the mechanistic link that was established between NIRv and the product of FPAR times *fesc* (Fig. 3) makes NIRv an attractive choice for studies related to GPP estimation and SIF[81,83,152,153].

Potential artefacts must be carefully taken care of to avoid biased interpretations of the underlying ecological processes resulting from the use of the incorrect data. Due to sensor degradation, the analysis and interpretation of the interannual variations and long-term trends in VIs remained challenging until the inter-calibration of AVHRR with MODIS became feasible after

2000 during the overlapping period[103]. The newer versions of VI products should theoretically be more accurate than the older ones[110]. Spectral response function normalizations are recommended for multi-sensor VI harmonizations[99]. The BRDF correction by the kernel-driven model is recommended especially if the BRDF varies seasonally and latitudinally in the analysis[120]. If uncertainties from sensor calibration[109], atmospheric, BRDF and topographic effects[134] are a serious issue to be reduced, ratio-based VIs are more recommended than difference-based VIs, while ratio-based VIs could be sensitive to snow/soil background[130] and scale effects[58]. For the spatial aggregation, it is highly recommended to firstly aggregate the single-band reflectance to coarse resolution, and then calculate VIs such as NDVI and EVI, instead of aggregating the high-resolution VIs directly, just to avoid the scaling effect over heterogeneous surfaces due to possible nonlinear formula of VIs[58].

Identifying dominant variables and potential signal contamination sources in specific ecosystems are also important for the correct use of VIs. For example, for temperate evergreen forests, the structure and chlorophyll in winter may not vary much, while physiologically-associated VIs such as PRI and CCI which are more sensitive to light use efficiency should be more suitable[50,51]. Tropical rainforest could be more vulnerable to atmosphere and optical signal saturation impacts[114] (EVI is more recommended instead of NDVI), savanna and shrubland with sparse vegetation are more sensitive to soil backgrounds[25] (EVI and NIRv are recommended), Artic region with high latitudes is vulnerable to large solar zenith angle and ice/snow backgrounds[130] (PPI, EVI2 and NIRv with BRDF correction are recommended), while mountainous regions such as the Tibetan Plateau with rugged terrain is vulnerable to not only ice/snow but also topographic and shadowing effects[142] (topographic normalizations including the empirical, semi-empirical and physically-based methods[154] are recommended).

8. Future directions

VIs with the spectral, angular, spatial and temporal information are classic remote sensing products with rich research history. Because of their simplicity and robustness, we envision they will continue to be heavily used in the foreseeable future. Looking forward, we identified a few research opportunities and challenges below that may advance the use of VIs for the more accurate and timely monitoring of terrestrial ecosystems from space.

8.1 Multi-sensor VI harmonization

Multi-sensor fusion of observations from multiple sensors/satellites can improve the spatio-temporal resolution and continuity as well as the timespan of VIs, such as Sentinel-2 and Landsat-8[155], which may greatly enhance their applicability. Ongoing efforts are devoted to developing fusion algorithms[156-159] and datasets[118,160,161] for producing long-term gap-free VIs at relatively high resolutions. However, land surface heterogeneity[162] and BRDF effects[117] remain to be major scientific challenges and issues to be resolved for producing fused VI products. The atmospheric correction also deserves greater attention, because even under the same solar angle, VIs differ depending on the fraction of diffuse radiation which differs at the overpassing times of different sensors/satellites. Sensor calibration drift and degradation are also critical challenges for the fusion of VI data from similar sensors on multiple satellites or multiple sensors on different satellites such as AVHRR and MODIS, in producing decadal datasets and analyses[103,104].

8.2 Synergistic use with novel metrics

Most VIs are good proxies of vegetation biophysical properties and to a limited extent represent vegetation functioning. Some novel remote sensing indicators, such as Solar-Induced chlorophyll Fluorescence (SIF)[163-166], could provide valuable complementary information. SIF captures some of the vegetation physiological information, and thus responds to the onset of environmental conditions and stresses earlier than VIs[167]. SIF can track the photosynthetic seasonality in evergreen species in cold environments where red-NIR VIs showed no changes[168]. Besides, SIF is rarely impacted by soil because green vegetation is the only source of SIF.

However, the existing SIF retrievals have poor spatial resolution, infrequent revisiting time, low signal to noise ratio, and a relatively short history of measurements[169]. New sensors/satellites will continue enhancing the capability for SIF measurement, but complementary VIs such as NIRv provide far better spatial and temporal resolutions. Understanding the intrinsic linkage between SIF and VIs is the key for the synergistic use for scientific applications, and one possible useful direction is to study the shared characteristics of SIF and VIs. In recent studies, far-red SIF normalized by Photosynthetically Active Radiation (SIF/PAR) and NIRv has been demonstrated to share the same *fesc* in the radiative transfer process[81,170] (Box 1). Thus, under low-stress conditions with stable fluorescence yield (Φ_F), NIRv and SIF/PAR are expected to be strongly correlated under the same sun-target-sensor geometry (Fig. S1). NIRv radiance (NDVI×NIR radiance) or NIRvP (NIRv×PAR) and SIF should be even more strongly related than NIRv and SIF/PAR as the common radiation factor further enhances the underlying relationship[4,82,152]. The similarity between NIRv and SIF implies that VIs could be used as structural proxies for SIF because they have a longer data record. For example, MODIS EVI has been used to generate a global SIF product (GOSIF; 2000-2020) from OCO-2 SIF soundings[171]. Combining NIRv with SIF during times of the overlapping data has great potential to isolate the unique physiological responses of SIF as NIRv can be used to normalize the dominant canopy structure effects[152,172].

Microwave vegetation indices derived from different frequency and polarization combinations are more sensitive to the woody part of the vegetation than NDVI[173], and are potential approaches to derive vegetation optical depth (VOD)[174]. VOD describes vegetation extinction effects in the microwave spectrum and is increasingly used for estimating parameters of vegetation water content and the aboveground biomass[175,176]. VOD has the advantage of being unaffected by the clouds and less sensitive to the water in the atmosphere, which is important especially for cloudy and humid tropical regions such as the Amazon and Congo rainforests[175,177]. VOD has been reported to have a saturation point with higher biomass values than NDVI[177]. Optical VIs with a higher spatial resolution can contribute to the downscaling of VOD, while VOD can help to improve the temporal observing frequency over cloudy and humid regions and seasons.

8.3 New remote sensing missions

The widely used red-NIR VIs which are sensitive to canopy structure and chlorophyll content do not directly contain the LUE information, which can be captured to some degree by several VIs such as PRI[49], CCI[5] and GCC[50,51] from emerging hyperspectral or multispectral remote sensing capabilities. In addition, hyperspectral data with more spectral information can be beneficial for the disentangling of the pure vegetation and soil reflectance contributions in the mixed pixel spectrum, by the newly proposed NIRvH[153]. The next generation of VIs aim at the reduction of soil/snow/ice background effects, reduced BRDF impact and reduced signal-saturation. Such hyperspectral remote sensing capability has been limited at the global scale and relatively fine spatial resolution. However, these limitations will be addressed with the emerging and forthcoming spaceborne hyperspectral satellite missions such as the HiSUI, PRISMA, EnMap, CHIME, DESIS, GeoCarb and SBG. New opportunities to further improve temporal characteristics of traditional VIs will also be provided by the new-generation geostationary satellites, such as GOES, Himawari and GEO-KOMPSAT, as well as the unique DSCOVR position at the Sun-Earth L1 Lagrange Point. They provide higher observing frequency that support not only the diurnal variations of ecosystem processes[178], but also the seasonality of greenness in cloudy and humid regions such as Amazon compared to polar-orbiting satellites[179,180].

9. Summary

This review summarizes inherent features of several widely used VIs and some factors contributing to consistencies and inconsistencies among them that may lead to controversies resulting from their inappropriate use in scientific studies and other applications. Factors such as the formulation of VIs, sensor characteristics, product version, compositing algorithms, QA/QC, atmospheric and topographic conditions, and sun-target-sensor geometries all impact VIs and their appropriate use. We further highlight that improper use of QA/QC flags attached to VIs could be an important source of uncertainty and pitfall in their use, and offer a few guidance and recommendations for the appropriate use of VIs. Mathematical analysis suggests that NIRv, EVI, EVI2 and DVI have similar radiative transfer features and are strongly linearly correlated with each other, while NDVI behaves differently as a ratio-based VI and is more impacted by soil background. NIRv, EVI, EVI2 and DVI can reproduce the results of each other in most cases because of their similarity.

Finally, we strongly recommend that future studies using VIs should be conducted with clear focus on interpretation of VIs, and using more than one *in-situ* dataset for verification when possible, to render greater confidence in their findings and conclusions. It would also be important to provide a detailed documentation of the key processing steps mentioned above to facilitate the interpretation and reproducibility of VI-based results. Ideally, the programming code should also be provided or made available when requested, and where feasible, the final VI dataset should be stored in a publicly accessible repository or cloud storage such as Google Earth Engine for ease of access [181]. In particular, the documentation should include relevant information on the application of QA/QC levels as well as any other processing steps such as spatio-temporal aggregation, additional quality and outlier filtering or other corrections applied to the original data. Providing such detailed technical information on VI products might be a promising strategy as then the documentation would be straightforward to find and also citable via a doi linked to a given dataset that is available for the user community. The technical review and recommendations presented here are intended to further advance the use of VIs in scientific studies and reduce any confusion and inconsistencies due to their improper use, considering the continued record length of existing capabilities, such as MODIS and VIIRS instruments, and emerging new ones, such as HiSUI, PRISMA and EnMap.

References

1. Bannari, A., Morin, D., Bonn, F. & Huete, A. A review of vegetation indices. *Remote sensing reviews* **13**, 95-120 (1995).
2. Gao, X., Huete, A. R., Ni, W. & Miura, T. Optical–biophysical relationships of vegetation spectra without background contamination. *Remote sensing of environment* **74**, 609-620 (2000).
3. Huete, A. R. A soil-adjusted vegetation index (SAVI). *Remote sensing of environment* **25**, 295-309 (1988).
4. Badgley, G., Field, C. B. & Berry, J. A. Canopy near-infrared reflectance and terrestrial photosynthesis. *Science Advances* **3**, e1602244 (2017).
5. Gamon, J. A. *et al.* A remotely sensed pigment index reveals photosynthetic phenology in evergreen conifers. *Proceedings of the National Academy of Sciences* **113**, 13087-13092 (2016).
6. Joiner, J. *et al.* Estimation of terrestrial global gross primary production (GPP) with satellite data-driven models and eddy covariance flux data. *Remote Sensing* **10**, 1346 (2018).

7 Piao, S. *et al.* Characteristics, drivers and feedbacks of global greening. *Nature Reviews Earth & Environment* **1**, 14-27 (2020).
8 Tian, F. *et al.* Evaluating temporal consistency of long-term global NDVI datasets for trend analysis. *Remote Sensing of Environment* **163**, 326-340 (2015).
9 Fan, X. & Liu, Y. A global study of NDVI difference among moderate-resolution satellite sensors. *ISPRS Journal of Photogrammetry and Remote Sensing* **121**, 177-191 (2016).
10 AghaKouchak, A. *et al.* Remote sensing of drought: Progress, challenges and opportunities. *Reviews of Geophysics* **53**, 452-480 (2015).
11 Anyamba, A. & Tucker, C. J. Historical perspective of AVHRR NDVI and vegetation drought monitoring. *Remote sensing of drought: Innovative monitoring approaches* **23**, 20 (2012).
12 Veraverbeke, S. *et al.* Hyperspectral remote sensing of fire: State-of-the-art and future perspectives. *Remote Sensing of Environment* **216**, 105-121 (2018).
13 Houborg, R., Fisher, J. B. & Skidmore, A. K. Advances in remote sensing of vegetation function and traits. *International Journal of Applied Earth Observation and Geoinformation* **43**, 1-6 (2015).
14 Tucker, C. J. Red and photographic infrared linear combinations for monitoring vegetation. *Remote Sensing of Environment* **8**, 127-150, doi:http://dx.doi.org/10.1016/0034-4257(79)90013-0 (1979).
15 Rouse, J. W., Haas, R. H., Schell, J. A. & Deering, D. W. Monitoring vegetation systems in the Great Plains with ERTS. *NASA special publication* **351**, 309 (1974).
16 Rouse, J. W., Haas, R. H., Schell, J. A., Deering, D. W. & Harlan, J. C. Monitoring the vernal advancement and retrogradation (green wave effect) of natural vegetation. *NASA/GSFC Type III Final Report, Greenbelt, Md* **371** (1974).
17 Gutman, G., Skakun, S. & Gitelson, A. Revisiting the use of red and near-infrared reflectances in vegetation studies and numerical climate models. *Science of Remote Sensing* **4**, 100025 (2021).
18 Jackson, R. D. & Huete, A. R. Interpreting vegetation indices. *Preventive veterinary medicine* **11**, 185-200 (1991).
19 Richardson, A. J. & Wiegand, C. Distinguishing vegetation from soil background information. *Photogrammetric engineering and remote sensing* **43**, 1541-1552 (1977).
20 Baret, F., Guyot, G. & Major, D. in *12th Canadian Symposium on Remote Sensing Geoscience and Remote Sensing Symposium.* 1355-1358 (IEEE).
21 Qi, J., Chehbouni, A., Huete, A. R., Kerr, Y. H. & Sorooshian, S. A modified soil adjusted vegetation index. *Remote sensing of environment* **48**, 119-126 (1994).
22 Chen, J. M. Evaluation of vegetation indices and a modified simple ratio for boreal applications. *Canadian Journal of Remote Sensing* **22**, 229-242 (1996).
23 Brown, L., Chen, J. M., Leblanc, S. G. & Cihlar, J. A shortwave infrared modification to the simple ratio for LAI retrieval in boreal forests: An image and model analysis. *Remote sensing of environment* **71**, 16-25 (2000).
24 Pinty, B. & Verstraete, M. GEMI: a non-linear index to monitor global vegetation from satellites. *Vegetatio* **101**, 15-20 (1992).
25 Huete, A. *et al.* Overview of the radiometric and biophysical performance of the MODIS vegetation indices. *Remote Sensing of Environment* **83**, 195-213, doi:http://dx.doi.org/10.1016/S0034-4257(02)00096-2 (2002).
26 Kaufman, Y. J. & Tanre, D. Atmospherically resistant vegetation index (ARVI) for EOS-MODIS. *IEEE transactions on Geoscience and Remote Sensing* **30**, 261-270 (1992).
27 Jiang, Z., Huete, A. R., Didan, K. & Miura, T. Development of a two-band enhanced vegetation index without a blue band. *Remote sensing of Environment* **112**, 3833-3845 (2008).

28 Jin, H. & Eklundh, L. A physically based vegetation index for improved monitoring of plant phenology. *Remote Sensing of Environment* **152**, 512-525, doi:10.1016/j.rse.2014.07.010 (2014).

29 Yang, P., van der Tol, C., Campbell, P. K. & Middleton, E. M. Fluorescence Correction Vegetation Index (FCVI): A physically based reflectance index to separate physiological and non-physiological information in far-red sun-induced chlorophyll fluorescence. *Remote sensing of environment* **240**, 111676 (2020).

30 Badgley, G., Anderegg, L. D., Berry, J. A. & Field, C. B. Terrestrial gross primary production: Using NIRV to scale from site to globe. *Global change biology* **25**, 3731-3740 (2019).

31 Camps-Valls, G. *et al.* A unified vegetation index for quantifying the terrestrial biosphere. *Science Advances* **7**, eabc7447 (2021).

32 Roberts, D. A., Roth, K. L. & Perroy, R. L. 14 hyperspectral vegetation indices. *Hyperspectral remote sensing of vegetation* **309** (2016).

33 Gitelson, A. A., Vina, A., Ciganda, V., Rundquist, D. C. & Arkebauer, T. J. Remote estimation of canopy chlorophyll content in crops. *Geophysical Research Letters* **32** (2005).

34 Gitelson, A. & Merzlyak, M. N. Spectral reflectance changes associated with autumn senescence of Aesculus hippocastanum L. and Acer platanoides L. leaves. Spectral features and relation to chlorophyll estimation. *Journal of plant physiology* **143**, 286-292 (1994).

35 Dash, J. & Curran, P. The MERIS terrestrial chlorophyll index. *International Journal of Remote Sensing* **25**, 5403-5413 (2004).

36 Penuelas, J., Baret, F. & Filella, I. Semi-empirical indices to assess carotenoids/chlorophyll a ratio from leaf spectral reflectance. *Photosynthetica* **31**, 221-230 (1995).

37 Peñuelas, J., Gamon, J., Fredeen, A., Merino, J. & Field, C. Reflectance indices associated with physiological changes in nitrogen-and water-limited sunflower leaves. *Remote sensing of Environment* **48**, 135-146 (1994).

38 Merzlyak, M. N., Gitelson, A. A., Chivkunova, O. B. & Rakitin, V. Y. Non‐destructive optical detection of pigment changes during leaf senescence and fruit ripening. *Physiologia plantarum* **106**, 135-141 (1999).

39 Gitelson, A. A., Merzlyak, M. N. & Chivkunova, O. B. Optical properties and nondestructive estimation of anthocyanin content in plant leaves. *Photochemistry and photobiology* **74**, 38-45 (2001).

40 van den Berg, A. K. & Perkins, T. D. Nondestructive estimation of anthocyanin content in autumn sugar maple leaves. *HortScience* **40**, 685-686 (2005).

41 Gamon, J. & Surfus, J. Assessing leaf pigment content and activity with a reflectometer. *The New Phytologist* **143**, 105-117 (1999).

42 Gao, B.-C. NDWI—A normalized difference water index for remote sensing of vegetation liquid water from space. *Remote sensing of environment* **58**, 257-266 (1996).

43 Xiao, X., Boles, S., Liu, J., Zhuang, D. & Liu, M. Characterization of forest types in Northeastern China, using multi-temporal SPOT-4 VEGETATION sensor data. *Remote Sensing of Environment* **82**, 335-348 (2002).

44 Xiao, X. *et al.* Satellite-based modeling of gross primary production in an evergreen needleleaf forest. *Remote sensing of environment* **89**, 519-534 (2004).

45 Yilmaz, M. T., Hunt Jr, E. R. & Jackson, T. J. Remote sensing of vegetation water content from equivalent water thickness using satellite imagery. *Remote Sensing of Environment* **112**, 2514-2522 (2008).

46 Cheng, Y.-B., Ustin, S. L., Riaño, D. & Vanderbilt, V. C. Water content estimation from hyperspectral images and MODIS indexes in Southeastern Arizona. *Remote Sensing of Environment* **112**, 363-374 (2008).

47 Serrano, L., Penuelas, J. & Ustin, S. L. Remote sensing of nitrogen and lignin in Mediterranean vegetation from AVIRIS data: Decomposing biochemical from structural signals. *Remote sensing of Environment* **81**, 355-364 (2002).

48 Filella, I. *et al.* PRI assessment of long-term changes in carotenoids/chlorophyll ratio and short-term changes in de-epoxidation state of the xanthophyll cycle. *International Journal of Remote Sensing* **30**, 4443-4455 (2009).

49 Gamon, J., Penuelas, J. & Field, C. A narrow-waveband spectral index that tracks diurnal changes in photosynthetic efficiency. *Remote Sensing of environment* **41**, 35-44 (1992).

50 Cheng, R. *et al.* Decomposing reflectance spectra to track gross primary production in a subalpine evergreen forest. *Biogeosciences* **17**, 4523-4544 (2020).

51 Seyednasrollah, B. *et al.* Seasonal variation in the canopy color of temperate evergreen conifer forests. *New Phytologist* **229**, 2586-2600 (2021).

52 Merton, R. in *Proceedings of the Seventh Annual JPL Airborne Earth Science Workshop.* 12-16.

53 Naidu, R. A., Perry, E. M., Pierce, F. J. & Mekuria, T. The potential of spectral reflectance technique for the detection of Grapevine leafroll-associated virus-3 in two red-berried wine grape cultivars. *Computers and Electronics in Agriculture* **66**, 38-45 (2009).

54 Chen, Y. *et al.* Generation and evaluation of LAI and FPAR products from Himawari-8 advanced Himawari imager (AHI) data. *Remote Sensing* **11**, 1517 (2019).

55 Zhu, Z. *et al.* Global Data Sets of Vegetation Leaf Area Index (LAI)3g and Fraction of Photosynthetically Active Radiation (FPAR)3g Derived from Global Inventory Modeling and Mapping Studies (GIMMS) Normalized Difference Vegetation Index (NDVI3g) for the Period 1981 to 2011. *Remote Sensing* **5**, 927-948, doi:10.3390/rs5020927 (2013).

56 Liu, Y., Liu, R. & Chen, J. M. Retrospective retrieval of long-term consistent global leaf area index (1981–2011) from combined AVHRR and MODIS data. *Journal of Geophysical Research* **117**, doi:10.1029/2012jg002084 (2012).

57 Croft, H. *et al.* The global distribution of leaf chlorophyll content. *Remote Sensing of Environment* **236**, 111479 (2020).

58 Jiang, Z. *et al.* Analysis of NDVI and scaled difference vegetation index retrievals of vegetation fraction. *Remote sensing of environment* **101**, 366-378 (2006).

59 Haboudane, D., Miller, J. R., Pattey, E., Zarco-Tejada, P. J. & Strachan, I. B. Hyperspectral vegetation indices and novel algorithms for predicting green LAI of crop canopies: Modeling and validation in the context of precision agriculture. *Remote sensing of environment* **90**, 337-352 (2004).

60 Wu, C., Wang, L., Niu, Z., Gao, S. & Wu, M. Nondestructive estimation of canopy chlorophyll content using Hyperion and Landsat/TM images. *International Journal of Remote Sensing* **31**, 2159-2167 (2010).

61 Wang, R. & Gamon, J. A. Remote sensing of terrestrial plant biodiversity. *Remote Sensing of Environment* **231**, 111218 (2019).

62 Ustin, S. L. & Gamon, J. A. Remote sensing of plant functional types. *New Phytologist* **186**, 795-816 (2010).

63 Hilker, T. *et al.* Vegetation dynamics and rainfall sensitivity of the Amazon. *Proceedings of the National Academy of Sciences* **111**, 16041-16046 (2014).

64 Zhang, Y., Commane, R., Zhou, S., Williams, A. P. & Gentine, P. Light limitation regulates the response of autumn terrestrial carbon uptake to warming. *Nature Climate Change* **10**, 739-743 (2020).

65 Weber, M. *et al.* Exploring the use of DSCOVR/EPIC satellite observations to monitor vegetation phenology. *Remote Sensing* **12**, 2384 (2020).

66 Wang, S., Zhang, Y., Ju, W., Qiu, B. & Zhang, Z. Tracking the seasonal and inter-annual variations of global gross primary production during last four decades using

satellite near-infrared reflectance data. *Science of the Total Environment* **755**, 142569 (2021).

67 Tian, F. *et al.* Calibrating vegetation phenology from Sentinel-2 using eddy covariance, PhenoCam, and PEP725 networks across Europe. *Remote Sensing of Environment* **260**, 112456 (2021).

68 Yin, G., Verger, A., Filella, I., Descals, A. & Peñuelas, J. Divergent estimates of forest photosynthetic phenology using structural and physiological vegetation indices. *Geophysical Research Letters* **47**, e2020GL089167 (2020).

69 Qin, Y. *et al.* Carbon loss from forest degradation exceeds that from deforestation in the Brazilian Amazon. *Nature Climate Change* **11**, 442-448 (2021).

70 Samanta, A. *et al.* Amazon forests did not green ‐ up during the 2005 drought. *Geophysical research letters* **37** (2010).

71 Shi, Y., Huang, W., Luo, J., Huang, L. & Zhou, X. Detection and discrimination of pests and diseases in winter wheat based on spectral indices and kernel discriminant analysis. *Computers and Electronics in Agriculture* **141**, 171-180 (2017).

72 Zhang, Z., Liu, M., Liu, X. & Zhou, G. A new vegetation index based on multitemporal Sentinel-2 images for discriminating heavy metal stress levels in rice. *Sensors* **18**, 2172 (2018).

73 Yengoh, G. T., Dent, D., Olsson, L., Tengberg, A. E. & Tucker III, C. J. *Use of the Normalized Difference Vegetation Index (NDVI) to assess Land degradation at multiple scales: current status, future trends, and practical considerations*. (Springer, 2015).

74 Potter, C. S. *et al.* Terrestrial ecosystem production: a process model based on global satellite and surface data. *Global Biogeochemical Cycles* **7**, 811-841 (1993).

75 Running, S. W. *et al.* A continuous satellite-derived measure of global terrestrial primary production. *Bioscience* **54**, 547-560 (2004).

76 Yuan, W. *et al.* Deriving a light use efficiency model from eddy covariance flux data for predicting daily gross primary production across biomes. *Agricultural and Forest Meteorology* **143**, 189-207 (2007).

77 Chen, M. *et al.* Quantification of terrestrial ecosystem carbon dynamics in the conterminous United States combining a process-based biogeochemical model and MODIS and AmeriFlux data. *Biogeosciences* **8**, 2665-2688 (2011).

78 Xiao, J. *et al.* A continuous measure of gross primary production for the conterminous United States derived from MODIS and AmeriFlux data. *Remote sensing of environment* **114**, 576-591 (2010).

79 Jiang, C., Guan, K., Wu, G., Peng, B. & Wang, S. A daily, 250 m, and real-time gross primary productivity product (2000–present) covering the Contiguous United States. *Earth Syst. Sci. Data Discuss.* **2020**, 1-28 (2020).

80 Schubert, P. *et al.* Modeling GPP in the Nordic forest landscape with MODIS time series data—Comparison with the MODIS GPP product. *Remote Sensing of Environment* **126**, 136-147 (2012).

81 Zeng, Y. *et al.* A practical approach for estimating the escape ratio of near-infrared solar-induced chlorophyll fluorescence. *Remote Sensing of Environment* **232**, 111209 (2019).

82 Baldocchi, D. D. *et al.* Outgoing Near Infrared Radiation from Vegetation Scales with Canopy Photosynthesis Across a Spectrum of Function, Structure, Physiological Capacity and Weather. *Journal of Geophysical Research: Biogeosciences*, e2019JG005534 (2020).

83 Dechant, B. *et al.* Canopy structure explains the relationship between photosynthesis and sun-induced chlorophyll fluorescence in crops. *Remote Sensing of Environment* **241**, 111733 (2020).

84 Rahman, A. F., Gamon, J. A., Fuentes, D. A., Roberts, D. A. & Prentiss, D. Modeling spatially distributed ecosystem flux of boreal forest using hyperspectral

indices from AVIRIS imagery. *Journal of Geophysical Research: Atmospheres* **106**, 33579-33591 (2001).
85 Wang, S. *et al.* Recent global decline of CO2 fertilization effects on vegetation photosynthesis. *Science* **370**, 1295-1300 (2020).
86 Zhu, Z. *et al.* Comment on "Recent global decline of CO2 fertilization effects on vegetation photosynthesis". *Science* **373**, eabg5673 (2021).
87 Huang, M. *et al.* Air temperature optima of vegetation productivity across global biomes. *Nature ecology & evolution* **3**, 772-779 (2019).
88 Doughty, R. *et al.* Small anomalies in dry-season greenness and chlorophyll fluorescence for Amazon moist tropical forests during El Niño and La Niña. *Remote Sensing of Environment* **253**, 112196 (2021).
89 Wigneron, J.-P. *et al.* Tropical forests did not recover from the strong 2015–2016 El Niño event. *Science advances* **6**, eaay4603 (2020).
90 Huang, N. *et al.* Spatial and temporal variations in global soil respiration and their relationships with climate and land cover. *Science advances* **6**, eabb8508 (2020).
91 Huang, N., He, J.-S. & Niu, Z. Estimating the spatial pattern of soil respiration in Tibetan alpine grasslands using Landsat TM images and MODIS data. *Ecological Indicators* **26**, 117-125 (2013).
92 Neale, C. M., Gonzalez‐Dugo, M. P., Serrano‐Perez, A., Campos, I. & Mateos, L. Cotton canopy reflectance under variable solar zenith angles: Implications of use in evapotranspiration models. *Hydrological Processes* **35**, e14162 (2021).
93 Chen, J. M. & Liu, J. Evolution of evapotranspiration models using thermal and shortwave remote sensing data. *Remote Sensing of Environment* **237**, 111594 (2020).
94 Glenn, E. P., Huete, A. R., Nagler, P. L. & Nelson, S. G. Relationship between remotely-sensed vegetation indices, canopy attributes and plant physiological processes: What vegetation indices can and cannot tell us about the landscape. *Sensors* **8**, 2136-2160 (2008).
95 Cui, Y., Jia, L. & Fan, W. Estimation of actual evapotranspiration and its components in an irrigated area by integrating the Shuttleworth-Wallace and surface temperature-vegetation index schemes using the particle swarm optimization algorithm. *Agricultural and Forest Meteorology* **307**, 108488 (2021).
96 Glenn, E. P., Neale, C. M., Hunsaker, D. J. & Nagler, P. L. Vegetation index‐based crop coefficients to estimate evapotranspiration by remote sensing in agricultural and natural ecosystems. *Hydrological Processes* **25**, 4050-4062 (2011).
97 French, A. N. *et al.* Satellite-based NDVI crop coefficients and evapotranspiration with eddy covariance validation for multiple durum wheat fields in the US Southwest. *Agricultural Water Management* **239**, 106266 (2020).
98 Fensholt, R. & Proud, S. R. Evaluation of earth observation based global long term vegetation trends—Comparing GIMMS and MODIS global NDVI time series. *Remote sensing of Environment* **119**, 131-147 (2012).
99 Trishchenko, A. P., Cihlar, J. & Li, Z. Effects of spectral response function on surface reflectance and NDVI measured with moderate resolution satellite sensors. *Remote Sensing of Environment* **81**, 1-18 (2002).
100 Ustin, S. L. & Middleton, E. M. Current and near-term advances in Earth observation for ecological applications. *Ecological processes* **10**, 1-57 (2021).
101 Wang, D. *et al.* Impact of sensor degradation on the MODIS NDVI time series. *Remote Sensing of Environment* **119**, 55-61 (2012).
102 Zhang, Y., Song, C., Band, L. E., Sun, G. & Li, J. Reanalysis of global terrestrial vegetation trends from MODIS products: Browning or greening? *Remote Sensing of Environment* **191**, 145-155 (2017).

103 Bhatt, R. *et al.* A consistent AVHRR visible calibration record based on multiple methods applicable for the NOAA degrading orbits. Part I: Methodology. *Journal of Atmospheric and Oceanic Technology* **33**, 2499-2515 (2016).

104 Frankenberg, C., Yin, Y., Byrne, B., He, L. & Gentine, P. COMMENT ON "RECENT GLOBAL DECLINE OF CO2 FERTILIZATION EFFECTS ON VEGETATION PHOTOSYNTHESIS". *Science* **373**, eabg2947, doi:10.1126/science.abg2947 (2021).

105 Los, S. O. Estimation of the ratio of sensor degradation between NOAA AVHRR channels 1 and 2 from monthly NDVI composites. *IEEE Transactions on Geoscience and Remote Sensing* **36**, 206-213 (1998).

106 Jiang, C. *et al.* Inconsistencies of interannual variability and trends in long‐term satellite leaf area index products. *Global Change Biology* **23**, 4133-4146 (2017).

107 de Beurs, K. M. & Henebry, G. M. Trend analysis of the Pathfinder AVHRR Land (PAL) NDVI data for the deserts of Central Asia. *IEEE Geoscience and Remote Sensing Letters* **1**, 282-286 (2004).

108 Wang, Z. *et al.* Large discrepancies of global greening: Indication of multi-source remote sensing data. *Global Ecology and Conservation*, e02016 (2022).

109 Miura, T., Huete, A. R. & Yoshioka, H. Evaluation of sensor calibration uncertainties on vegetation indices for MODIS. *Geoscience and Remote Sensing, IEEE Transactions on* **38**, 1399-1409 (2000).

110 Lyapustin, A. *et al.* Scientific impact of MODIS C5 calibration degradation and C6+ improvements. *Atmospheric Measurement Techniques* **7**, 4353-4365 (2014).

111 Buchhorn, M., Raynolds, M. K. & Walker, D. A. Influence of BRDF on NDVI and biomass estimations of Alaska Arctic tundra. *Environmental Research Letters* **11**, 125002 (2016).

112 Morton, D. C. *et al.* Amazon forests maintain consistent canopy structure and greenness during the dry season. *Nature* **506**, 221-224, doi:10.1038/nature13006 (2014).

113 Fensholt, R., Sandholt, I., Proud, S. R., Stisen, S. & Rasmussen, M. O. Assessment of MODIS sun-sensor geometry variations effect on observed NDVI using MSG SEVIRI geostationary data. *International Journal of Remote Sensing* **31**, 6163-6187 (2010).

114 Saleska, S. R. *et al.* Dry-season greening of Amazon forests. *Nature* **531**, E4-E5 (2016).

115 Lyapustin, A. I. *et al.* Multi-angle implementation of atmospheric correction for MODIS (MAIAC): 3. Atmospheric correction. *Remote Sensing of Environment* **127**, 385-393 (2012).

116 Norris, J. R. & Walker, J. J. Solar and sensor geometry, not vegetation response, drive satellite NDVI phenology in widespread ecosystems of the western United States. *Remote Sensing of Environment* **249**, 112013 (2020).

117 Roy, D. P. *et al.* A general method to normalize Landsat reflectance data to nadir BRDF adjusted reflectance. *Remote Sensing of Environment* **176**, 255-271 (2016).

118 Schaaf, C. B. *et al.* First operational BRDF, albedo nadir reflectance products from MODIS. *Remote sensing of Environment* **83**, 135-148 (2002).

119 Didan, K., Munoz, A. B., Solano, R. & Huete, A. MODIS vegetation index user's guide (MOD13 series). *University of Arizona: Vegetation Index and Phenology Lab* (2015).

120 Wang, Z., Schaaf, C. B., Sun, Q., Shuai, Y. & Román, M. O. Capturing rapid land surface dynamics with Collection V006 MODIS BRDF/NBAR/Albedo (MCD43) products. *Remote sensing of environment* **207**, 50-64 (2018).

121 Saleska, S. R., Didan, K., Huete, A. R. & Da Rocha, H. R. Amazon forests green-up during 2005 drought. *Science* **318**, 612-612 (2007).

122 Vargas, M., Miura, T., Shabanov, N. & Kato, A. An initial assessment of Suomi NPP VIIRS vegetation index EDR. *Journal of Geophysical Research: Atmospheres* **118**, 12,301-312,316 (2013).
123 Kobayashi, H. & Dye, D. G. Atmospheric conditions for monitoring the long-term vegetation dynamics in the Amazon using normalized difference vegetation index. *Remote Sensing of Environment* **97**, 519-525 (2005).
124 Jiang, C. & Fang, H. GSV: a general model for hyperspectral soil reflectance simulation. *International Journal of Applied Earth Observation and Geoinformation* **83**, 101932 (2019).
125 Verrelst, J., Schaepman, M. E., Malenovský, Z. & Clevers, J. G. Effects of woody elements on simulated canopy reflectance: Implications for forest chlorophyll content retrieval. *Remote Sensing of Environment* **114**, 647-656 (2010).
126 Huete, A. & Tucker, C. Investigation of soil influences in AVHRR red and near-infrared vegetation index imagery. *International journal of remote sensing* **12**, 1223-1242 (1991).
127 Farrar, T., Nicholson, S. & Lare, A. The influence of soil type on the relationships between NDVI, rainfall, and soil moisture in semiarid Botswana. II. NDVI response to soil oisture. *Remote sensing of Environment* **50**, 121-133 (1994).
128 Huete, A. & Warrick, A. Assessment of vegetation and soil water regimes in partial canopies with optical remotely sensed data. *Remote Sensing of Environment* **32**, 155-167 (1990).
129 Wang, C. *et al.* A snow-free vegetation index for improved monitoring of vegetation spring green-up date in deciduous ecosystems. *Remote sensing of environment* **196**, 1-12 (2017).
130 Myers-Smith, I. H. *et al.* Complexity revealed in the greening of the Arctic. *Nature Climate Change* **10**, 106-117 (2020).
131 Shen, M. *et al.* No evidence of continuously advanced green-up dates in the Tibetan Plateau over the last decade. *Proceedings of the National Academy of Sciences* **110**, E2329-E2329 (2013).
132 Grover, V. I., Borsdorf, A., Breuste, J., Tiwari, P. C. & Frangetto, F. W. *Impact of global changes on mountains: responses and adaptation*. (CRC Press, 2014).
133 Hao, D. *et al.* Modeling anisotropic reflectance over composite sloping terrain. *IEEE Transactions on Geoscience and Remote Sensing* **56**, 3903-3923 (2018).
134 Matsushita, B., Yang, W., Chen, J., Onda, Y. & Qiu, G. Sensitivity of the enhanced vegetation index (EVI) and normalized difference vegetation index (NDVI) to topographic effects: a case study in high-density cypress forest. *Sensors* **7**, 2636-2651 (2007).
135 Wen, J. *et al.* Characterizing land surface anisotropic reflectance over rugged terrain: A review of concepts and recent developments. *Remote Sensing* **10**, 370 (2018).
136 Friedl, M. A., Davis, F. W., Michaelsen, J. & Moritz, M. Scaling and uncertainty in the relationship between the NDVI and land surface biophysical variables: An analysis using a scene simulation model and data from FIFE. *Remote Sensing of Environment* **54**, 233-246 (1995).
137 Tan, B. *et al.* The impact of gridding artifacts on the local spatial properties of MODIS data: Implications for validation, compositing, and band-to-band registration across resolutions. *Remote Sensing of Environment* **105**, 98-114 (2006).
138 Wolfe, R. E. *et al.* Achieving sub-pixel geolocation accuracy in support of MODIS land science. *Remote Sensing of Environment* **83**, 31-49 (2002).
139 Ferreira, M. P. *et al.* Retrieving structural and chemical properties of individual tree crowns in a highly diverse tropical forest with 3D radiative transfer modeling and imaging spectroscopy. *Remote Sensing of Environment* **211**, 276-291 (2018).

140 Huete, A. R. *et al.* Amazon rainforests green‐up with sunlight in dry season. *Geophysical research letters* **33** (2006).
141 Herrmann, S. M. & Tappan, G. G. Vegetation impoverishment despite greening: A case study from central Senegal. *Journal of Arid Environments* **90**, 55-66 (2013).
142 Wang, X. *et al.* No consistent evidence for advancing or delaying trends in spring phenology on the Tibetan Plateau. *Journal of Geophysical Research: Biogeosciences* **122**, 3288-3305 (2017).
143 Donnelly, A., Yu, R. & Liu, L. Comparing in situ spring phenology and satellite-derived start of season at rural and urban sites in Ireland. *International Journal of Remote Sensing* **42**, 7821-7841 (2021).
144 Templ, B. *et al.* Pan European Phenological database (PEP725): a single point of access for European data. *International journal of biometeorology* **62**, 1109-1113 (2018).
145 Fu, Y. H. *et al.* Declining global warming effects on the phenology of spring leaf unfolding. *Nature* **526**, 104-107 (2015).
146 Chen, X. & Yang, Y. Observed earlier start of the growing season from middle to high latitudes across the Northern Hemisphere snow-covered landmass for the period 2001–2014. *Environmental Research Letters* **15**, 034042 (2020).
147 Alatorre, L. C. *et al.* Temporal changes of NDVI for qualitative environmental assessment of mangroves: shrimp farming impact on the health decline of the arid mangroves in the Gulf of California (1990–2010). *Journal of Arid Environments* **125**, 98-109 (2016).
148 Jacquemoud, S. & Baret, F. PROSPECT: A model of leaf optical properties spectra. *Remote sensing of environment* **34**, 75-91 (1990).
149 Wu, S. *et al.* Quantifying leaf optical properties with spectral invariants theory. *Remote Sensing of Environment* **253**, 112131 (2021).
150 Wang, Z. *et al.* Mapping foliar functional traits and their uncertainties across three years in a grassland experiment. *Remote Sensing of Environment* **221**, 405-416 (2019).
151 Van Leeuwen, W. & Huete, A. Effects of standing litter on the biophysical interpretation of plant canopies with spectral indices. *Remote sensing of Environment* **55**, 123-138 (1996).
152 Dechant, B. *et al.* NIRvP: A robust structural proxy for sun-induced chlorophyll fluorescence and photosynthesis across scales. *Remote Sensing of Environment* **268**, 112763 (2022).
153 Zeng, Y. *et al.* Estimating near-infrared reflectance of vegetation from hyperspectral data. *Remote Sensing of Environment* **267**, 112723 (2021).
154 Hantson, S. & Chuvieco, E. Evaluation of different topographic correction methods for Landsat imagery. *International Journal of Applied Earth Observation and Geoinformation* **13**, 691-700 (2011).
155 Zhang, H. K. *et al.* Characterization of Sentinel-2A and Landsat-8 top of atmosphere, surface, and nadir BRDF adjusted reflectance and NDVI differences. *Remote sensing of environment* **215**, 482-494 (2018).
156 Gao, F., Masek, J., Schwaller, M. & Hall, F. On the blending of the Landsat and MODIS surface reflectance: Predicting daily Landsat surface reflectance. *IEEE Transactions on Geoscience and Remote sensing* **44**, 2207-2218 (2006).
157 Zhu, X. *et al.* A flexible spatiotemporal method for fusing satellite images with different resolutions. *Remote Sensing of Environment* **172**, 165-177 (2016).
158 Luo, Y., Guan, K. & Peng, J. STAIR: A generic and fully-automated method to fuse multiple sources of optical satellite data to generate a high-resolution, daily and cloud-/gap-free surface reflectance product. *Remote Sensing of Environment* **214**, 87-99 (2018).

159 Houborg, R. & McCabe, M. F. Daily Retrieval of NDVI and LAI at 3 m Resolution via the Fusion of CubeSat, Landsat, and MODIS Data. *Remote Sensing* **10**, 890 (2018).
160 Kimm, H. *et al.* Deriving high-spatiotemporal-resolution leaf area index for agroecosystems in the US Corn Belt using Planet Labs CubeSat and STAIR fusion data. *Remote Sensing of Environment* **239**, 111615 (2020).
161 Claverie, M. *et al.* The Harmonized Landsat and Sentinel-2 surface reflectance data set. *Remote Sensing of Environment* **219**, 145-161 (2018).
162 Kong, J. *et al.* Evaluation of four image fusion NDVI products against in-situ spectral-measurements over a heterogeneous rice paddy landscape. *Agricultural and Forest Meteorology* **297**, 108255 (2021).
163 Köhler, P. *et al.* Global retrievals of solar ‐ induced chlorophyll fluorescence with TROPOMI: First results and intersensor comparison to OCO ‐ 2. *Geophysical Research Letters* **45**, 10,456-410,463 (2018).
164 Sun, Y. *et al.* OCO-2 advances photosynthesis observation from space via solar-induced chlorophyll fluorescence. *Science* **358** (2017).
165 Joiner, J., Yoshida, Y., Vasilkov, A. & Middleton, E. First observations of global and seasonal terrestrial chlorophyll fluorescence from space. *Biogeosciences* **8**, 637-651 (2011).
166 Frankenberg, C. *et al.* New global observations of the terrestrial carbon cycle from GOSAT: Patterns of plant fluorescence with gross primary productivity. *Geophysical Research Letters* **38** (2011).
167 Qiu, B., Ge, J., Guo, W., Pitman, A. J. & Mu, M. Responses of Australian dryland vegetation to the 2019 heat wave at a subdaily scale. *Geophysical Research Letters* **47**, e2019GL086569 (2020).
168 Magney, T. S. *et al.* Mechanistic evidence for tracking the seasonality of photosynthesis with solar-induced fluorescence. *Proceedings of the National Academy of Sciences* **116**, 11640-11645 (2019).
169 Guanter, L. *et al.* Potential of the TROPOspheric Monitoring Instrument (TROPOMI) onboard the Sentinel-5 Precursor for the monitoring of terrestrial chlorophyll fluorescence. *Atmospheric Measurement Techniques* **8**, 1337-1352 (2015).
170 Knyazikhin, Y. *et al.* Hyperspectral remote sensing of foliar nitrogen content. *Proceedings of the National Academy of Sciences* **110**, E185-E192 (2013).
171 Li, X. & Xiao, J. A global, 0.05-degree product of solar-induced chlorophyll fluorescence derived from OCO-2, MODIS, and reanalysis data. *Remote Sensing* **11**, 517 (2019).
172 Zeng, Y. *et al.* Combining near-infrared radiance of vegetation and fluorescence spectroscopy to detect effects of abiotic changes and stresses. *Remote Sensing of Environment* **270**, 112856 (2022).
173 Shi, J. *et al.* Microwave vegetation indices for short vegetation covers from satellite passive microwave sensor AMSR-E. *Remote sensing of environment* **112**, 4285-4300 (2008).
174 Talebiesfandarani, S. *et al.* Microwave vegetation index from multi-angular observations and its application in vegetation properties retrieval: Theoretical modelling. *Remote Sensing* **11**, 730 (2019).
175 Wigneron, J.-P. *et al.* SMOS-IC data record of soil moisture and L-VOD: Historical development, applications and perspectives. *Remote Sensing of Environment* **254**, 112238 (2021).
176 Zhang, Y., Zhou, S., Gentine, P. & Xiao, X. Can vegetation optical depth reflect changes in leaf water potential during soil moisture dry-down events? *Remote Sensing of Environment* **234**, 111451 (2019).
177 Frappart, F. *et al.* Global monitoring of the vegetation dynamics from the Vegetation Optical Depth (VOD): A review. *Remote Sensing* **12**, 2915 (2020).

178 Xiao, J., Fisher, J. B., Hashimoto, H., Ichii, K. & Parazoo, N. C. Emerging satellite observations for diurnal cycling of ecosystem processes. *Nature Plants*, 1-11 (2021).

179 Hashimoto, H. *et al.* New generation geostationary satellite observations support seasonality in greenness of the Amazon evergreen forests. *Nature communications* **12**, 1-11 (2021).

180 Somkuti, P. *et al.* Solar-induced chlorophyll fluorescence from the Geostationary Carbon Cycle Observatory (GeoCarb): An extensive simulation study. *Remote Sensing of Environment* **263**, 112565 (2021).

181 Gorelick, N. *et al.* Google Earth Engine: Planetary-scale geospatial analysis for everyone. *Remote sensing of Environment* **202**, 18-27 (2017).

182 Baret, F. & Guyot, G. Potentials and limits of vegetation indices for LAI and APAR assessment. *Remote sensing of environment* **35**, 161-173 (1991).

183 Broge, N. H. & Leblanc, E. Comparing prediction power and stability of broadband and hyperspectral vegetation indices for estimation of green leaf area index and canopy chlorophyll density. *Remote sensing of environment* **76**, 156-172 (2001).

184 Nemani, R., Pierce, L., Running, S. & Band, L. Forest ecosystem processes at the watershed scale: sensitivity to remotely-sensed leaf area index estimates. *International journal of remote sensing* **14**, 2519-2534 (1993).

185 Chamard, P. *et al.* Utilisation des bandes spectrales du vert et du rouge pour une meilleure évaluation des formations végétales actives. *Télédétection et cartographie*, 203-209 (1991).

186 Gitelson, A. A. *et al.* Remote estimation of leaf area index and green leaf biomass in maize canopies. *Geophysical research letters* **30** (2003).

187 Sripada, R. P., Heiniger, R. W., White, J. G. & Weisz, R. Aerial color infrared photography for determining late‐season nitrogen requirements in corn. *Agronomy Journal* **97**, 1443-1451 (2005).

188 Gitelson, A. A., Kaufman, Y. J. & Merzlyak, M. N. Use of a green channel in remote sensing of global vegetation from EOS-MODIS. *Remote sensing of Environment* **58**, 289-298 (1996).

189 Kim, M. S. *The Use of Narrow Spectral Bands for Improving Remote Sensing Estimations of Fractionally Absorbed Photosynthetically Active Radiation*, (1994).

190 Daughtry, C. S., Walthall, C., Kim, M., De Colstoun, E. B. & McMurtrey Iii, J. Estimating corn leaf chlorophyll concentration from leaf and canopy reflectance. *Remote sensing of Environment* **74**, 229-239 (2000).

191 Haboudane, D., Miller, J. R., Tremblay, N., Zarco-Tejada, P. J. & Dextraze, L. Integrated narrow-band vegetation indices for prediction of crop chlorophyll content for application to precision agriculture. *Remote sensing of environment* **81**, 416-426 (2002).

192 Blackburn, G. A. Spectral indices for estimating photosynthetic pigment concentrations: a test using senescent tree leaves. *International Journal of remote sensing* **19**, 657-675 (1998).

193 Gitelson, A. A., Zur, Y., Chivkunova, O. B. & Merzlyak, M. N. Assessing carotenoid content in plant leaves with reflectance spectroscopy. *Photochemistry and photobiology* **75**, 272-281 (2002).

194 Gitelson, A. A., Keydan, G. P. & Merzlyak, M. N. Three‐band model for noninvasive estimation of chlorophyll, carotenoids, and anthocyanin contents in higher plant leaves. *Geophysical research letters* **33** (2006).

195 Steele, M. R., Gitelson, A. A., Rundquist, D. C. & Merzlyak, M. N. Nondestructive estimation of anthocyanin content in grapevine leaves. *American Journal of Enology and Viticulture* **60**, 87-92 (2009).

196 Peñuelas, J., Pinol, J., Ogaya, R. & Filella, I. Estimation of plant water concentration by the reflectance water index WI (R900/R970). *International journal of remote sensing* **18**, 2869-2875 (1997).

197 Daughtry, C. S. Discriminating crop residues from soil by shortwave infrared reflectance. *Agronomy Journal* **93**, 125-131 (2001).

198 Daughtry, C. S., Hunt, E., Doraiswamy, P. & McMurtrey, J. Remote sensing the spatial distribution of crop residues. (2005).

199 Richardson, A. D., Braswell, B. H., Hollinger, D. Y., Jenkins, J. P. & Ollinger, S. V. Near-surface remote sensing of spatial and temporal variation in canopy phenology. *Ecological Applications* **19**, 1417-1428, doi:10.1890/08-2022.1 (2009).

200 Chen, B., Jin, Y. & Brown, P. An enhanced bloom index for quantifying floral phenology using multi-scale remote sensing observations. *ISPRS Journal of Photogrammetry and Remote Sensing* **156**, 108-120 (2019).

Figures, tables and boxes

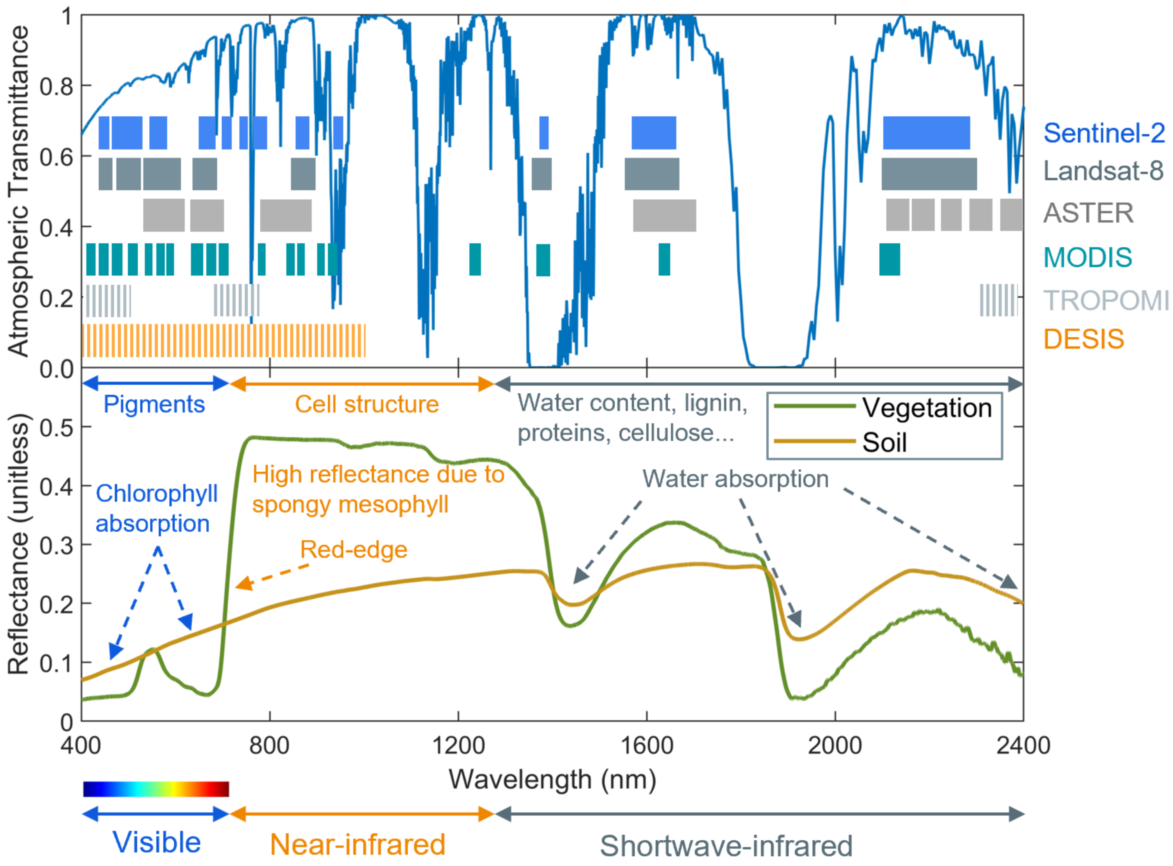

Fig. 1. The vegetation and soil spectrum across wavelengths to design vegetation indices. The spectral response range in the atmospheric window of a few widely used satellites are also included[100]. The colored blocks and vertical lines in the top panel illustrate the spectral band range or band pass for each satellite sensor.

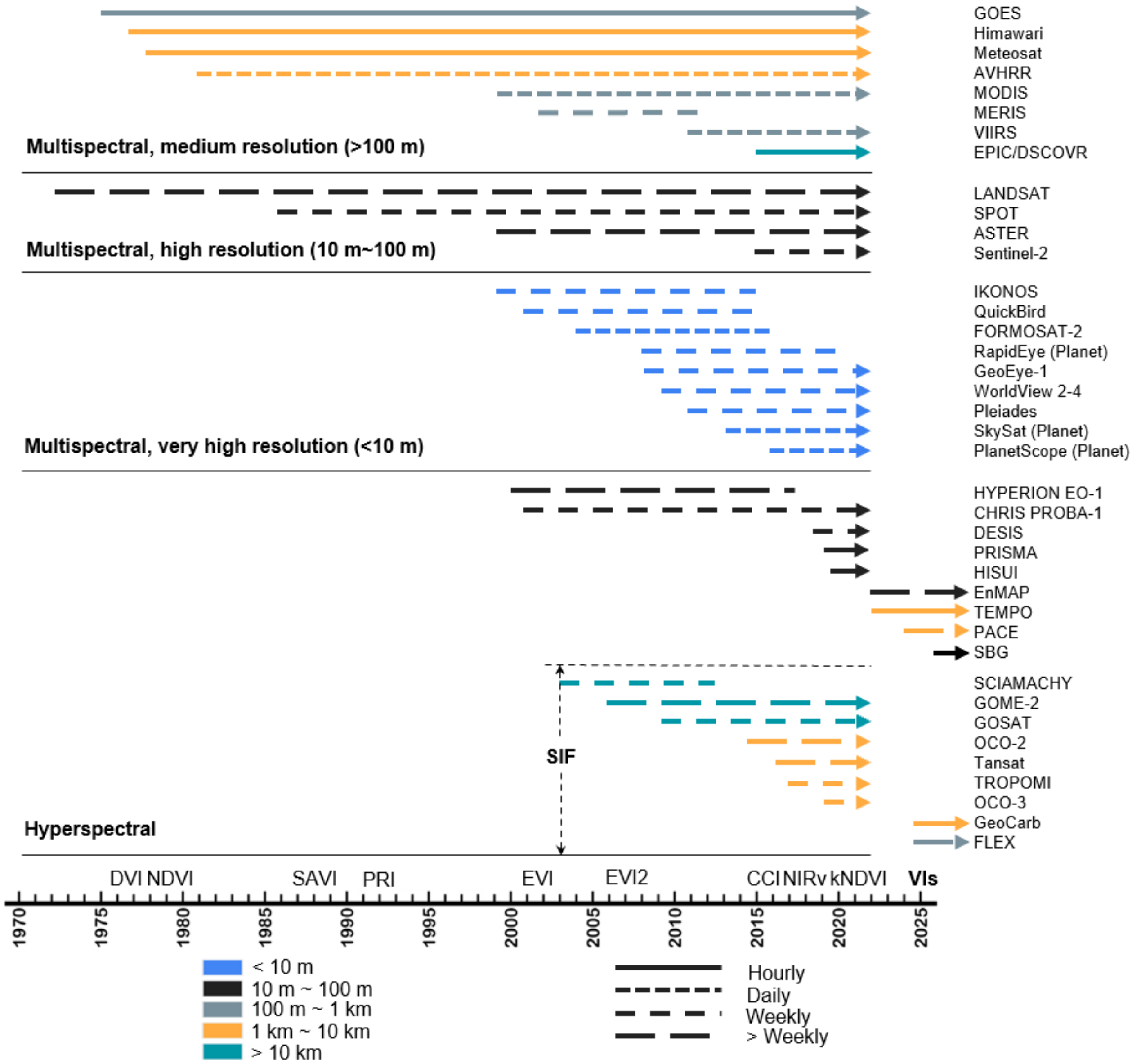

Fig. 2 The timeline of widely used satellites with the capability to derive VIs. The corresponding spatio-temporal resolutions are also included.

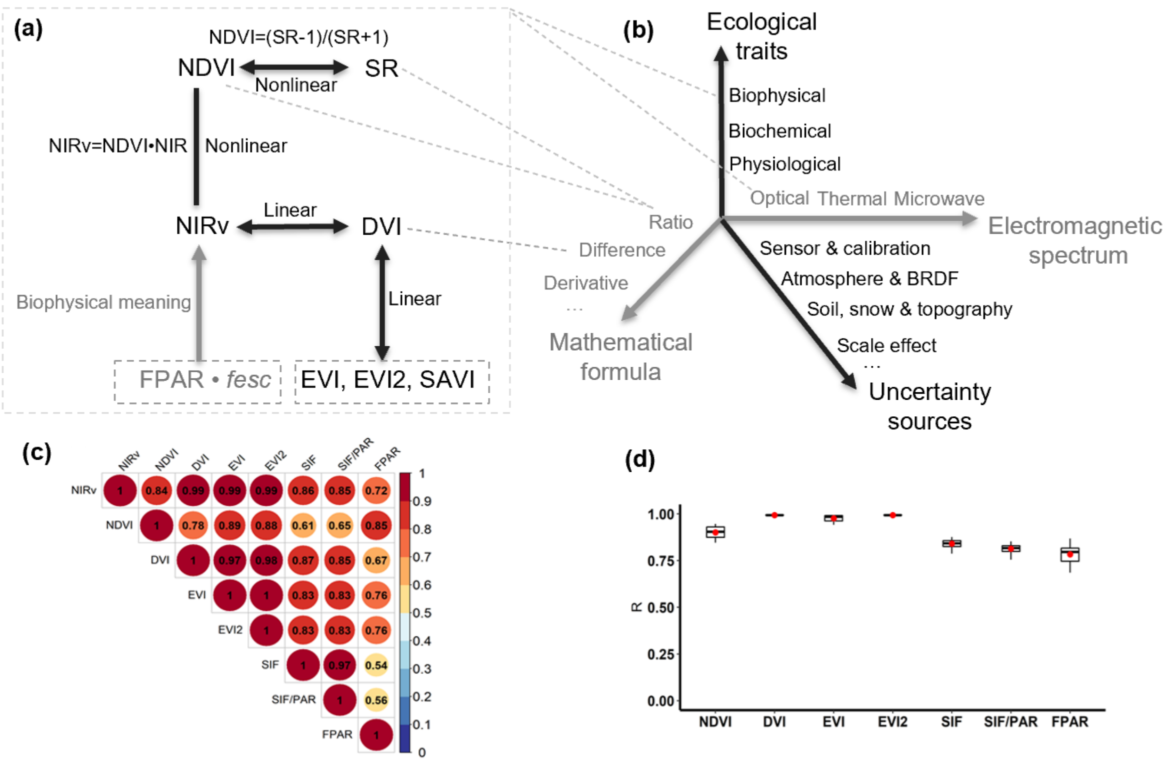

Fig. 3 The taxonomy, physical meaning and similarity of VIs. a| The biophysical interpretation and intrinsic linkage of several most widely used VIs in a variety of global-scale ecological studies. **b|** The taxonomy of VIs from four different dimensions: physics, mathematics, ecology and uncertainties. **c|** Global spatial correlations of monthly-averaged MODIS NIRv, DVI, EVI, EVI2, SIF, SIF/PAR (PAR-normalized SIF), NDVI and FPAR in August, 2018 and at 0.1° spatial resolution, considered as the peak growing month for most vegetation types. **d|** Global spatial correlations between MODIS NIRv and other remote sensing VIs during the 2018.03~2019.02 period since the origin of TROPOMI SIF, with the temporal resolution of 4 days and 0.1° spatial resolution. In the box plot, red circle refers to the mean value, boxes represent the interquartile ranges of the 25th (Q25) and 75th (Q75) percentiles, and whiskers cover the ranges of Q25 - 1.5·(Q75 - Q25) and Q75+1.5·(Q75 - Q25). The *R*s among NIRv, DVI, EVI and EVI2 were greater than 0.95, while the *R* between NDVI and other VIs ranged from 0.78 to 0.89. NDVI has a relatively larger *R* with FPAR, but has a weaker linear correlation with SIF than the other VIs. In the spatial aggregation, the red, NIR and blue reflectance was firstly averagely aggregated to 0.1 degrees, and then the VIs were calculated.

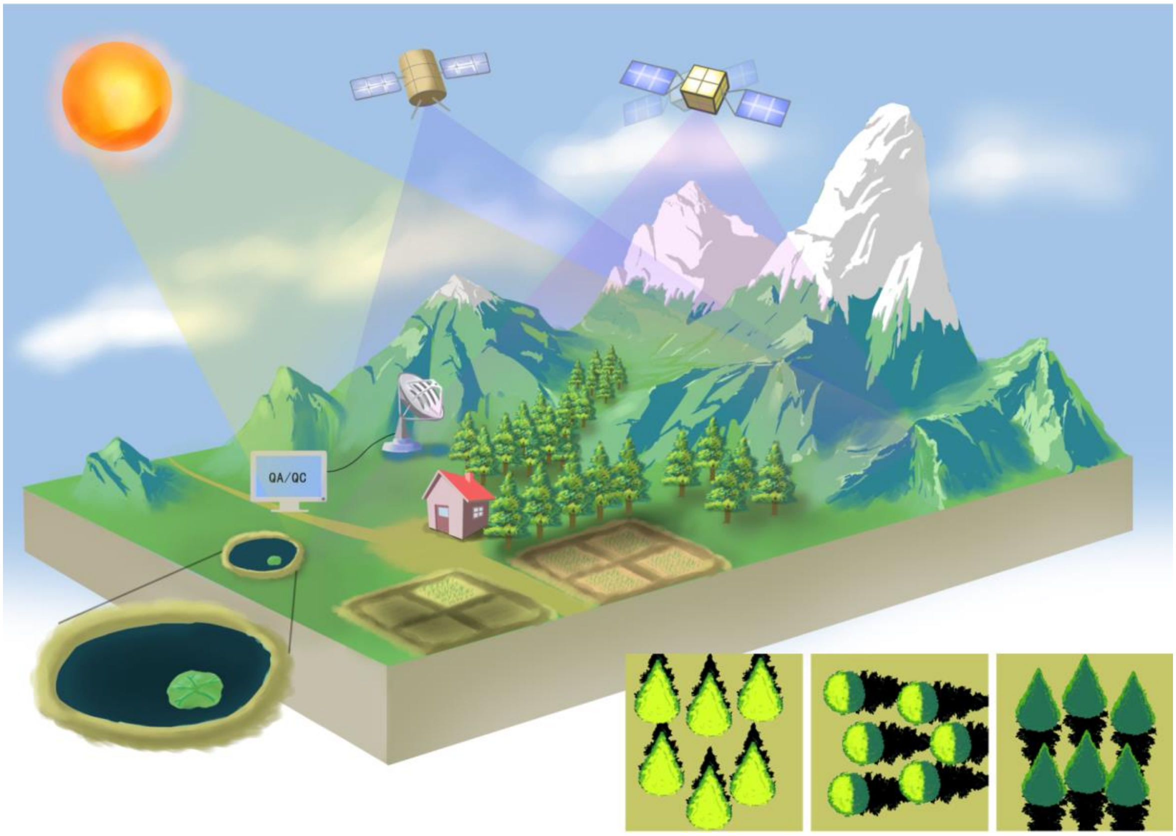

Fig. 4 A sketch map of VIs from satellite observations. Uncertainties come from different sensors and calibration, QA/QC flags and compositing algorithms, atmosphere and BRDF effects, soil/snow background and topography, and scale effects.

Table 1: **The widely used optical vegetation indices, spectral ranges and references**

Spectral space	Name and references	Abbreviation	Equation and derivation	Primary applications, advantages and disadvantages
Red-NIR	Simple Ratio[14]	SR	NIR/Red	Structure; Simple but sensitive to the atmospheric correction of the red band
Red-NIR	Normalized Difference Vegetation Index[14-16]	NDVI	$(NIR - Red)/(NIR + Red)$ $= (SR - 1)/(SR + 1)$ $= 1 - 2/(SR + 1)$	Structure; Simple but sensitive to the soil background variations
Red-NIR	Modified Simple Ratio[22]	MSR	$\frac{NIR/Red - 1}{\sqrt{NIR/Red + 1}}$	Structure; More linear relationship with canopy structure parameters
Red-NIR	Difference Vegetation Index[19]	DVI	$NIR - Red$	Structure; Simple but sensitive to the BRDF effect
Red-NIR	Global Environment Monitoring Index[24]	GEMI	$\eta \cdot (1 - 0.25 \cdot \eta) - \frac{Red - 0.125}{1 - Red}$ $\eta = \frac{2 \cdot (NIR^2 - Red^2) + 1.5 \cdot NIR + 0.5 \cdot Red}{NIR + Red + 0.5}$	Structure; Reduce the atmospheric perturbation effects, while maintain the vegetation information
Red-NIR	Perpendicular Vegetation Index[19]	PVI	$\sqrt{(NIR_{soil} - NIR_{veg})^2 + (Red_{soil} - Red_{veg})^2}$	Structure; Minimize the soil background influence but need the slope and intercept of the soil line
Red-NIR	Soil Adjusted Vegetation Index[3]	SAVI	$(1 + L) \cdot (NIR - Red)/(NIR + Red + L)$	Structure; Minimize the soil background influence but sensitive to the BRDF effect

Red-NIR	Modified SAVI[21]	MSAVI	$(2 \cdot NIR + 1 - \sqrt{(2 \cdot NIR + 1)^2 - 8 \cdot (NIR - Red)})/2$	Structure; Further minimize the soil background influence while increase the dynamic range of vegetation signal
Red-NIR	Transformed SAVI[20]	TSAVI	$a \cdot (NIR - a \cdot Red - b)/(a \cdot NIR + Red - a \cdot b)$	Structure; Minimize the soil background influence and work well for LAI and APAR estimations
Red-NIR	Adjusted TSAVI[182]	ATSAVI	$a \cdot (NIR - a \cdot Red - b)/[a \cdot NIR + Red - a \cdot b + 0.08 \cdot (1 + a^2)]$	Structure; Minimize the soil background influence and work well for LAI and APAR estimations
VIS-NIR	Atmospherically Resistant Vegetation Index[26]	ARVI	$(NIR - RB)/(NIR + RB)$, $RB = Red - \gamma \cdot (Blue - Red)$	Structure; Minimize the atmospheric effect and work better for vegetated surfaces than for soils, but need the blue band
VIS-NIR	Soil Adjusted and Atmospherically Resistant Vegetation Index[26]	SARVI	$(1 + L) \cdot (NIR - RB)/(NIR + RB + L)$, $RB = Red - \gamma \cdot (Blue - Red)$	Structure; Minimize both the soil and atmospheric effects, but need the blue band
VIS-NIR	Enhanced Vegetation Index[25]	EVI	$2.5 \cdot (NIR - Red)/(NIR + 6 \cdot Red - 7.5 \cdot Blue + 1)$	Structure; Minimize both the soil and atmospheric effects, while sensitive to the BRDF effect and need the blue band
Red-NIR	two-band EVI without the blue-band[27]	EVI2	$2.5 \cdot (NIR - Red)/(NIR + 2.4 \cdot Red + 1)$	Structure; Minimize the soil background influence and no need the blue band, while sensitive to the BRDF effect

Red-NIR	Near-Infrared Reflectance of vegetation[4]	NIRv	$NDVI \cdot NIR$	Structure; Minimize the soil background influence, while sensitive to the BRDF effect
VIS-NIR	Hyperspectral NIRv[153]	NIRvH	$NIR - Red - k(\lambda_{NIR} - \lambda_{Red})$	Structure; Further minimize the soil background influence, while sensitive to the BRDF effect
VIS-NIR	Fluorescence Correction Vegetation Index[29]	FCVI	$NIR - VIS$	Structure; Minimize the soil background influence, while sensitive to the BRDF effect
VIS-NIR	Kernel NDVI[31]	kNDVI	$\tanh(NDVI^2)$	Structure; Higher sensitivity to canopy structural parameters and GPP
VIS-NIR	Plant Phenology Index[28]	PPI	$-K \cdot \ln(\frac{M - DVI}{M - DVI_S})$	Structure; Linearly related to green LAI, less severely impacted by snow than NDVI and EVI, and work well for phenology at high latitudes, while need the soil DVI
VIS-NIR	Triangular Vegetation Index[183]	TVI	$0.5 \cdot [120 \cdot (R_{750} - R_{550}) - 200 \cdot (R_{670} - R_{550})]$	Structure; Biochemical: chlorophyll; Describe the radiation absorbed by the pigments
VIS-NIR	Modified Triangular Vegetation Index 1[59]	MTVI1	$1.2 \cdot [1.2 \cdot (R_{800} - R_{550}) - 2.5 \cdot (R_{670} - R_{550})]$	Structure; Insensitive to pigment changes, and better for LAI estimations than TVI
VIS-NIR	Modified Triangular Vegetation Index 2[59]	MTVI2	$1.5 \cdot [1.2 \cdot (R_{800} - R_{550}) - 2.5 \cdot (R_{670} - R_{550})] / \sqrt{(2 \cdot R_{800} + 1)^2 - (6 \cdot R_{800} - 5 \cdot \sqrt{R_{670}}) - 0.}$	Structure; Minimize both the soil background and chlorophyll effects, while sensitive to LAI and thus a good LAI predictor

VIS-NIR	Modified Chlorophyll Absorption Ratio Index 1[59]	MCARI1	$1.2 \cdot [2.5 \cdot (R_{800} - R_{670}) - 1.3 \cdot (R_{800} - R_{550})]$	Structure; Less sensitive to chlorophyll variations than MCARI, while sensitive to LAI changes
VIS-NIR	Modified Chlorophyll Absorption Ratio Index 2[59]	MCARI2	$1.5 \cdot [2.5 \cdot (R_{800} - R_{670}) - 1.3 \cdot (R_{800} - R_{550})] / \sqrt{(2 \cdot R_{800} + 1)^2 - (6 \cdot R_{800} - 5 \cdot \sqrt{R_{670}}) - 0.}$	Structure; Minimize both the soil background and chlorophyll effects, while sensitive to LAI and thus a good LAI predictor
VIS-NIR-MIR	MIR corrected NDVI[184]	NDVIc	$\mathrm{NDVI} \cdot (1 - \frac{\mathrm{MIR} - \mathrm{MIR_{min}}}{\mathrm{MIR_{max}} - \mathrm{MIR_{min}}})$	Structure; Considered the canopy closure and understory contribution in LAI estimations by leaf water absorption of open canopies
VIS-NIR-SWIR	Reduced SR[23]	RSR	$\mathrm{SR} \cdot (1 - \frac{\mathrm{SWIR} - \mathrm{SWIR_{min}}}{\mathrm{SWIR_{max}} - \mathrm{SWIR_{min}}})$	Structure; Increased the sensitivity and correlation to LAI than SR in boreal forests, while reduced the effect of background reflectance
Green-Red	Normalized Difference Greenness Index[185]	NDGI	$(Green - Red)/(Green + Red)$	Structure; Work well for identifying and mapping vegetation in inundated regions, no need the blue or NIR bands, and can work at PhenoCam imageries
Green-NIR	Green Chlorophyll Vegetation Index[186]	GCVI	$NIR/Green - 1$	Structure; Biochemical: chlorophyll; Depend on both LAI and chlorophyll concentration, and close relationship with LAI and green leaf biomass
Green-NIR	Green Difference Vegetation Index[187]	GDVI	$NIR - Green$	Biochemical: chlorophyll; Work well for predicting the late-season nitrogen requirement for corn

Green-NIR	Green Normalized Difference Vegetation Index[188]	GNDVI	$(NIR - Green)/(NIR + Green)$	Biochemical: chlorophyll; More sensitive to chlorophyll concentration than NDVI
Red edge-NIR	Red Edge Chlorophyll Index[33]	CIred-edge	$NIR/Re - 1$	Biochemical: chlorophyll; Linear relationship between the chlorophyll content in maize and soybean leaves with CIred-edge
Red edge -NIR	Red-edge NDVI[34]	NDVIre	$(NIR - RE)/(NIR + RE)$	Biochemical: chlorophyll; Directly proportional to chlorophyll and serve as indicators of leaf senescence
Red edge -NIR	MERIS Total Chlorophyll Index[35]	MTCI	$(R_{750} - R_{710})/((R_{710} - R_{680})$	Biochemical: chlorophyll; Correlate strongly with red-edge position and is sensitive to high values of chlorophyll content.
Red-Red edge	Chlorophyll Absorption Ratio Index[189,190]	CARI	$(R_{700} - R_{670}) - 0.2 \cdot (R_{700} - R_{550})$	Biochemical: chlorophyll; Minimize the effect of nonphotosynthetic materials in the FPAR estimations
Red-Red edge	Modified Chlorophyll Absorption in Reflectance Index[190]	MCARI	$[(R_{700} - R_{670}) - 0.2 \cdot (R_{700} - R_{550})] \cdot (R_{700}/R_{670})$	Biochemical: chlorophyll; Sensitive to leaf chlorophyll concentrations
Red-Red edge	Transformed Chlorophyll Absorption in Reflectance Index[191]	TCARI	$3 \cdot [(R_{700} - R_{670}) - 0.2 \cdot (R_{700} - R_{550}) \cdot (R_{700}/R_{670})]$	Biochemical: chlorophyll; Sensitive to chlorophyll over a wide range of variations, and is more sensitive to chlorophyll than MCARI

VIS-NIR	Pigment Specific Normalized Difference[192]	PSND	$(R_{800} - R_{675})/((R_{800} + R_{675})\ for\ Chl_a$; $(R_{800} - R_{650})/((R_{800} + R_{650})\ for\ Chl_b$; $(R_{800} - R_{500})/((R_{800} + R_{500})\ for\ Car$;	Biochemical: chlorophyll, carotenoid; Strong relation with chlorophyll, while poor relation with carotenoid
VIS-NIR	Pigment Specific Simple Ratio[192]	PSSR	$(R_{800}/R_{675})\ for\ Chl_a$; $(R_{800}/R_{650})\ for\ Chl_b$; $(R_{800}/R_{500})\ for\ Car$;	Biochemical: chlorophyll, carotenoid; Strong relation with chlorophyll, while poor relation with carotenoid
VIS-Red edge	Carotenoid Reflectance Index[193]	CRI	$1/R_{510} - 1/R_{550}$; $1/R_{510} - 1/R_{700}$	Biochemical: carotenoid; Remove the chlorophyll effect from the reflectance in the green edge range, and is sufficient to estimate the carotenoid content in plant leaves
VIS-Red edge	Plant Senescence Reflectance Index[38]	PSRI	$(R_{678} - R_{500})/R_{750}$	Biochemical: carotenoid, chlorophyll; Sensitive to the Car/Chl ratio, and can be used as a quantitative measure of leaf senescence/fruit ripening process
VIS	Normalized Pigments Chlorophyll Ratio Index[37]	NPCI	$(R_{680} - R_{430})/(R_{680} + R_{430})$	Biochemical: carotenoid, chlorophyll; Vary with the ratio of total pigments/Chl, indicative of plant phenology status
VIS-NIR	Structure Insensitive Pigment Index[36]	SIPI	$(R_{800} - R_{445})/((R_{800} - R_{680})$	Biochemical: carotenoid, chlorophyll a; Physiological; Minimize the confounding effects of the leaf surface and mesophyll structure, and provide the best semi-empirical estimation of the ratio of Car/Chla
Green-Red edge	Anthocyanin Reflectance Index[39]	ARI	$1/R_{550} - 1/R_{700}$	Biochemical: anthocyanin; An accurate estimation of anthocyanin accumulation

VIS-NIR	Modified Anthocyanin Reflectance Index[39,194]	MARI	$(1/R_{550} - 1/R_{700}) \cdot NIR$	Biochemical: anthocyanin; The best fit function with the Anthocyanin content, and yield accurate assessment
VIS	Red/Green Ratio Index[41]	RGRI	$Red/Green$	Biochemical: anthocyanin; Strongly related to pigment estimated by destructive sampling and spectrophotometric quantification
Green-NIR	Anthocyanin Content Index[40]	ACI	$\alpha_{Green}/\alpha_{NIR}$	Biochemical: anthocyanin; Linear relationship with total extractable anthocyanin content
Green-NIR	Modified Anthocyanin Content Index[195]	MACI	$NIR/Green$	Biochemical: anthocyanin, chlorophyll; Depends on three variables: chlorophyll, anthocyanin, and leaf thickness, and when the three vary independently, MACI becomes insensitive to anthocyanin.
NIR-SWIR	Normalized Difference Water Index[42]	NDWI	$\frac{NIR_{860} - SWIR_{1240}}{NIR_{860} + SWIR_{1240}}$	Biochemical: water content; Sensitive to vegetation water content changes, less sensitive to atmospheric effects than NDVI, while not completely remove the soil background reflectance effect as NDVI
NIR-SWIR	Land Surface Water Index[43,44]	LSWI	$\frac{R_{780\sim890} - R_{1580\sim1790}}{R_{780\sim890} + R_{1580\sim1790}}$	Biochemical: water content; A useful indicator for water content of evergreen needleleaf forest, useful for improving classification of cropland and forests, and improve the GPP estimations in the VPM model

NIR-SWIR	Normalized Difference Infrared Index[45]	NDII	$\frac{R_{850} - R_{1650}}{R_{850} + R_{1650}}$	Biochemical: water content; Related to canopy water content, linearly related to Equivalent Water Thickness (EWT) for corn, soybean and woodland
NIR-SWIR	Water Index[196]	WI	R_{900}/R_{970}	Biochemical: water content; Correlate with plant water concentration, and useful in evaluation of wild fire risk and drought
SWIR	Normalized Difference Lignin Index[47]	NDLI	$[\log(1/R_{1754}) - \log(1/R_{1680})]/[\log(1/R_{1754}) + \log(1/R_{1680})]$	Biochemical: lignin; Significantly correlate to foliar lignin concentration in green canopies, while unable to assess foliar or bulk canopy lignin in senescing vegetation
SWIR	Cellulose Absorption Index[197]	CAI	$100 \cdot [0.5 \cdot (R_{2019} + R_{2206}) - R_{2109}]$	Biochemical: cellulose; Positive for all crop residues, while all soils have negative values, and thus can discriminate crop residues from soil under dry and moist conditions
SWIR	Lignin Cellulose Absorption Index[198]	LCA	$100 \cdot [(R_{2185\sim2225} - R_{2145\sim2185}) + (R_{2185\sim2225} - R_{2295\sim2365})]$	Biochemical: lignin, cellulose; Linearly relate to crop residue cover with the R^2 higher than eight VIs in the evaluation
SWIR	Normalized Difference Nitrogen Index[47]	NDNI	$[\log(1/R_{1510}) - \log(1/R_{1680})]/[\log(1/R_{1510}) + \log(1/R_{1680})]$	Biochemical: nitrogen; Significantly correlate to foliar nitrogen concentration in green canopies, while unable to assess foliar or bulk canopy nitrogen in senescing vegetation

VIS	Photochemical Reflectance Index[49]	PRI	$(R_{531} - R_{570})/((R_{531} - R_{570})$	Physiological; Well track the diurnal changes of photosynthetic activity, but need to reduce complications associated with diurnal sun angle changes
VIS	Chlorophyll Carotenoid Index[5]	CCI	$\frac{Band_{11} - Band_{1}}{Band_{11} + Band_{1}}$	Physiological; Biochemical; Well track the seasonality of daily GPP and phenology for evergreen conifers at multiple spatial scales, and can be acquired at the global scale with MODIS data compared to PRI
VIS	Green Chromatic Coordinate[50,199]	GCC	$Green/(Red + Green + Blue)$	Physiological; Structure; Biochemical; Sensitive to changes in both carotenoid and chlorophyll, correlate well with GPP seasonality but less than CCI and PRI, and can be easily acquired using RGB imagery
Red edge	Red-edge Vegetation Stress Index[52]	RVSI	$(R_{714} + R_{752})/2 - R_{733}$	Physiological; Useful in the detection of stressed leaves in grapevine leafroll disease
VIS	Enhanced Bloom Index[200]	EBI	$\frac{Red + Green + Blue}{\frac{Green}{Blue} \cdot (Red - Blue + \varepsilon)}$	Physiological; Structure; Biochemical; Reduce the soil and green vegetation background noise, and can capture the flower information using RGB imagery from ground to satellites

Box 1: **Physical clarification of a few VIs and SIF on their linkages and differences**

DVI is defined as the difference between the NIR and Red bands[19]:

$$DVI = NIR - Red \qquad (1)$$

Here we demonstrate the linkage between NIRv and other VIs such as DVI, EVI and EVI2, by using DVI as the bridge among them. By definition, NIRv can be derived as the product of DVI and NIR/(NIR+Red)[4].

$$NIRv = NDVI \cdot NIR = \frac{NIR - Red}{NIR + Red} \cdot NIR = DVI \cdot \frac{NIR}{NIR + Red} \sim DVI \qquad (2)$$

$$EVI = 2.5 \cdot \frac{NIR - Red}{NIR + 6 \cdot Red - 7.5 \cdot Blue + 1} = DVI \cdot \frac{2.5}{NIR + 6 \cdot Red - 7.5 \cdot Blue + 1} \sim DVI \quad (3)$$

$$EVI2 = 2.5 \cdot \frac{NIR - Red}{NIR + 2.4 \cdot Red + 1} = DVI \cdot \frac{2.5}{NIR + 2.4 \cdot Red + 1} \sim DVI \quad (4)$$

Below we show the linkage and difference between NDVI, SR and SAVI. Note when L in SAVI is 0, SAVI is equal to NDVI.

$$NDVI = \frac{NIR - Red}{NIR + Red} = \frac{SR - 1}{SR + 1} = 1 - \frac{2}{SR + 1} \quad (5)$$

$$SR = NIR/Red \quad (6)$$

$$SAVI = (1 + L) \cdot \frac{NIR - Red}{NIR + Red + L} \quad (7)$$

Based on spectral invariants theory, NIRv and SIF/PAR can be modelled in similar formula[81]:

$$NIRv = FPAR \cdot \omega \cdot f_{esc} \quad (8)$$

$$SIF/PAR = FPAR \cdot \Phi_F \cdot f_{esc} \quad (9)$$

where *fesc* is the photon escape probability from the canopy, ω is the leaf single scattering albedo in the NIR band, which is close to 1 in the NIR band, and Φ_F is the fluorescence yield. Rearranging Eqs. 8 and 9 gives

$$NIRv: (SIF/PAR) = \omega : \Phi_F \qquad (10)$$

Glossary

AVHRR: Advanced Very High Resolution Radiometer

CHIME: Copernicus Hyperspectral Imaging Mission for the Environment

DESIS: DLR Earth Sensing Imaging Spectrometer

DSCOVR: Deep Space Climate Observatory

EnMap: Environmental Monitoring and Analysis Program

EPIC: Earth Polychromatic Imaging Camera

ETM+: Enhanced Thematic Mapper Plus

FLEX: FLuorescence EXplorer

GIMMS-3g: Global Inventory Modeling and Mapping Studies-3rd generation

GOES: Geostationary Operational Environmental Satellite

HiSUI: Hyper-spectral Imager SUIte

LTDR4: Long Term Data Record version 4

MAIAC: Multi-Angle Implementation of Atmospheric Correction

MERIS: MEdium Resolution Imaging Spectrometer

MODIS: MODerate resolution Imaging Spectroradiometer

MSG: Meteosat Second Generation

PACE: Plankton, Aerosol, Cloud, ocean Ecosystem

PRISMA: PRecursore IperSpettrale della Missione Applicativa

SBG: Surface Biology and Geology

SEVIRI: Spinning Enhanced Visible and Infrared Imager

SPOT-VGT: Systeme Pour l'Observation de la Terre VEGETATION

TEMPO: Tropospheric Emissions: Monitoring of Pollution

VIIRS: Visible Infrared Imaging Radiometer Suite

VIP3: Vegetation Index and Phenology version 3

Acknowledgements

This research was supported by the National Aeronautics and Space Administration (NASA) through Remote Sensing Theory and Arctic Boreal Vulnerability Experiment (ABoVE) grants 80NSSC21K0568 and NNH18ZDA001N granted to Min Chen. J. X. was supported by National Science Foundation (NSF) (Macrosystem Biology & NEON-Enabled Science program: DEB-2017870). Y. R. was supported by National Research Foundation of Korea (NRF-2019R1A2C2084626). The authors thank Grayson Badgley for the fruitful discussions on vegetation indices. The TROPOMI far-red daily SIF dataset[163] was acquired from ftp://fluo.gps.caltech.edu/data/tropomi provided by Philipp Köhler. The authors acknowledge the insightful comments and suggestions from the editors and three anonymous reviewers.

Author contributions

Y. Z., D. H., A. H., J. B., G. A. and M. C. wrote the synopsis and the initial draft of the manuscript. B. D., J. C., J. J., C. F., B. L., Y. R. and J. X. reviewed and edited the manuscript before submission. All authors made substantial contributions to the improvement of manuscript.

Competing interests

The authors declare no competing interests.